U-Pb zircon geochronology of rocks from west Central Sulawesi, Indonesia: Extension-related metamorphism and magmatism during the early stages of mountain building

Juliane Hennig [a,*], Robert Hall [a] and Richard A. Armstrong [b]

[a] *SE Asia Research Group, Department of Earth Sciences, Royal Holloway University of London, Egham, Surrey, TW20 0EX, UK*

[b] *Research School of Earth Sciences, Australian National University, Canberra, ACT, 0200, Australia*

* Corresponding author: *j.hennig@es.rhul.ac.uk*

Abstract

Sulawesi has generally been interpreted as the product of convergence in the Cretaceous and Cenozoic, and high mountains in west Central Sulawesi have been considered the product of magmatism and metamorphism related to Neogene collision. New SHRIMP and LA-ICP-MS U-Pb zircon dating of metamorphic and granitoid rocks has identified protoliths and sources of melts, and indicates an important role for extension. Schists, gneisses and granitoids have inherited Proterozoic, Paleozoic, Mesozoic and Paleogene zircons. Mesoproterozoic and Triassic age populations are similar to those from the Bird's Head region. Their protoliths included sediments and granitoids interpreted as part of an Australian-origin block. We suggest this rifted from the Australian margin of Gondwana in the Jurassic and accreted to Sundaland to form NW Sulawesi in the Late Cretaceous. Some metamorphic rocks have Cretaceous and/or Late Eocene magmatic zircons indicating metamorphism cannot be older than Late Eocene, and were not Australian-origin basement. Instead, they were metamorphosed in the Neogene after Sula Spur collision and subsequent major extension. Associated magmatism in west Central Sulawesi produced a K-rich shoshonitic (HK) suite in the Middle Miocene to Early Pliocene. A later episode of magmatism in the Late Miocene to Pliocene formed mainly shoshonitic to high-K calc-alkaline (CAK) rocks. I-type and silica-rich I-type granitoids and diorites of the CAK suite record a widespread short interval of magmatism between 8.5 and 4 Ma. Inherited zircon ages indicate the I-type

CAK rocks were the product of partial melting of the HK suite. S-type CAK magmatism between c. 5 and 2.5 Ma and zircon rim ages from gneisses record contemporaneous metamorphism that accompanied extension. Despite its position in a convergent setting in Indonesia, NW Sulawesi illustrates the importance of melting and metamorphism in an extensional setting during the early stages of mountain building.

Keywords: Sulawesi; Palu Metamorphic Complex; SHRIMP; LA-ICP-MS; Inner Banda block.

1. Introduction

Sulawesi is located in Eastern Indonesia in the region of convergence of the Indo-Australian, Eurasian and Philippine Sea plates. The island is the product of a complex tectonic history of terrane rifting and accretion, opening and closure of basins, subduction and extension. Western Sulawesi is the eastern part of Sundaland, which was assembled from Gondwana-derived continental fragments during the late Paleozoic and Mesozoic to form the southeast part of the Eurasian plate (e.g. Hutchison, 1973, 1989; Metcalfe, 1988, 1990, 1996, 2011; Hall & Morley, 2004). East Java and West Sulawesi are now considered to have been part of the Argoland terrane that rifted from the Australian margin during the Jurassic and accreted to the Sundaland margin in the Late Cretaceous (Smyth et al., 2007; Hall et al., 2009; Metcalfe, 2009; Hall, 2011; Hall & Sevastjanova, 2012). In the Eocene renewed northward subduction opened the Celebes Sea and initiated rifting of the Makassar Straits that now separate western Sulawesi from east Borneo (Hamilton, 1979; Weissel, 1980; Hall, 1996). Early Miocene collision of the NW promontory of Australia, the Sula Spur, with the Sulawesi North Arm volcanic arc led to the emplacement of the East Arm ophiolite (Parkinson, 1998a) and the addition of more continental crust to the Sundaland margin (Hall, 1996, 2002, 2012). Spakman and Hall (2010) proposed that subduction rollback into the Banda Embayment, which initiated at c.15-16 Ma (Pownall et al., 2013, 2014), caused the Sula Spur to extend and fragment as the slab rolled back eastwards and it is likely that the initiation of Banda rollback was associated with extension in Sulawesi (Hall, 2011, 2012).

Western Sulawesi includes a wide range of metamorphic, igneous and sedimentary rocks (Fig. 1). There are Cretaceous or Early Miocene subduction-related ultra-high pressure and high pressure metamorphic rocks (de Roever, 1947, 1955; Wakita et al., 1996; Parkinson et al., 1998; Kadarusman et al., 2001, 2002, 2005), Upper Cretaceous to Paleogene sedimentary and low-grade metasedimentary rocks (van Leeuwen & Muhardjo, 2005), Paleogene basic to intermediate volcanic and intrusive rocks (van Leeuwen & Muhardjo, 2005), Neogene granitoids and co-magmatic volcanic rocks (Priadi et al., 1994; Polvé et al., 1997; Elburg et al., 2003) as well as Pliocene to Pleistocene Celebes Molasse (Sarasin & Sarasin, 1901; van Leeuwen & Muhardjo, 2005).

Collisions in Sulawesi in the Late Cretaceous and Early Miocene of Australian-origin crust, including metasediments and metagranitoids, imply an old metamorphic basement in Western Sulawesi. Previous authors assigned the metamorphic rocks to this basement (e.g. van Leeuwen & Muhardjo, 2005), with metamorphism presumed to be of Paleozoic to Early Mesozoic age (Sopaheluwakan et al., 1995) or to be the result of subduction during the late Mesozoic (Parkinson et al., 1998). Little is known about the age, origin and protoliths of the metamorphic rocks or the magmatic and metamorphic history of the region. This study reports new results based on a field-based investigation of these rocks, accompanied by petrological and geochemical studies and U-Pb dating of zircons from igneous and metamorphic rocks from Western Sulawesi.

2. Stratigraphy

2.1 Metamorphic rocks

The Palu Metamorphic Complex (PMC) is a large area of metamorphic rocks in the Neck of Central Sulawesi (van Leeuwen & Muhardjo, 2005). Smaller areas of metamorphic rocks are found further south on the east side of the Palu-Koro Fault, where they are assigned to the Gumbasa Complex (Sukido et al., 1993) or the PMC (van Leeuwen & Muhardjo, 2005). There are other metamorphic rocks further to the east in the high mountain range between the Palolo and the Besoa Basins, which were not assigned to a named complex.

Rocks from the PMC are described as biotite- and amphibole-schists, paragneisses, granite-gneisses, granulites, amphibolites and marbles (Egeler, 1947; Sukamto, 1973;

van Leeuwen & Muhardjo, 2005). These rocks vary in composition, metamorphic grade and intensity of deformation. Biotite schists with abundant quartz lenses, enclosing irregular amphibolite bodies with sharp tectonic contacts, are dominant in the western part of the complex, whereas biotite gneisses, garnet-bearing gneisses, pyroxene gneisses and marbles were observed in the east part of the complex. Schists and gneisses are highly deformed and are partially melted in places.

Metamorphic rocks south of the PMC and east of the Palu-Koro Fault include biotite schists, sheared gneisses, garnet-sillimanite-cordierite granulites and migmatites as well as foliated to intensely sheared amphibolites, garnet amphibolites and amphibole-plagioclase gneisses based on field observations made during this study.

The protoliths and origin of all the metamorphic rocks in mid Central Sulawesi are poorly known. The different areas of metamorphic rocks (Fig. 1) were previously assumed to be different in age and possibly origin, and therefore subdivided into separate complexes (Sukido et al., 1993; van Leeuwen & Muhardjo, 2005). However, based on the similarity of lithologies observed in the field, and the new U-Pb zircon data presented in this paper (section 4), the terms for different complexes are used here only to refer to geographic regions.

2.2 Metasedimentary rocks

Sedimentary and metasedimentary rocks at various places in the Neck (Fig. 1) were assigned to the Tinombo Formation (Sukamto, 1973; Ratman, 1976). Similar rocks occur in mid Sulawesi and were assigned to the Latimojong Formation south of Palu (Sukido et al., 1993; Simandjuntak et al., 1997). Lithologies observed in both formations include mudstones, siltstones, sandstones, conglomerates, slates, marls and limestones. Some of the rocks in the Neck are folded and have a very low-grade greenschist facies overprint.

The depositional age of the sedimentary rocks is poorly known and is based on palaeontological evidence. Pelagic carbonates and nummulitic limestones on the east side of the Neck south of Tinombo (Fig. 1) and further north near Tolitoli (Fig. 1) were used to date the Tinombo Formation as Middle Eocene to earliest Miocene (Sukamto, 1973; van Leeuwen et al., 1994; van Leeuwen & Muhardjo, 2005).

2.3 Basic to intermediate volcanic rocks

Basaltic to rhyolitic rocks are found in the weakly metamorphosed greenschist facies metasediments of the Tinombo Formation in the Neck region (Ahlburg, 1913; Brouwer, 1934; Elburg et al., 2003; van Leeuwen & Muhardjo, 2005). The volcanic rocks in the Neck and west of Palu include basaltic to andesitic lavas, and volcaniclastics, of tholeiitic and calc-alkaline composition (Priadi et al., 1994; Polvé et al., 1997; Elburg et al., 2003; van Leeuwen & Muhardjo, 2005). Locally, the basaltic rocks are deformed and have a poorly developed schistosity. Basalts and dolerites in the southern part of the Neck have sharp tectonic contacts with the metamorphic rocks of the PMC.

Similar rocks continue into the North Arm where they form the main part of the Papayato Volcanics (Fig. 1) (Sukamto, 1973; Ratman, 1976; Apandi, 1977; Kavalieris et al., 1992). The Latimojong Formation typically lacks a volcanic component. Therefore, the metasediments and the volcanic rocks of the Tinombo and Papayato Formations are separated from the Latimojong Formation in this study.

The volcanic rocks are poorly dated. Limited K-Ar dating of whole-rocks and feldspars have yielded ages from 34.5 ± 0.8 Ma to 52.7 ± 1.4 Ma (Polvé et al., 1997).

2.4 Granitoids and diorites

Granitoid and diorite rocks are abundant in Central Sulawesi and form large intrusive bodies in the Neck and to the east and west of the Palu-Koro Fault in mid Central Sulawesi (Sukamto, 1973; Ratman, 1976; Kavalieris et al., 1992; Sukido et al., 1993; van Leeuwen et al., 1994; Priadi et al., 1994; Simandjuntak et al., 1997; Polvé et al., 1997; Elburg et al., 2003; van Leeuwen & Muhardjo, 2005). Small stocks and dykes cross-cut various lithologies in Central Sulawesi.

2.4.1 Paleogene granitic stocks and sills

Sills and stocks of granodiorites, diorites and two-mica granites crop out in the Neck and to the west of Palu. They are found close to the Paleogene volcanic rocks and were assigned to the 'Tinombo Intrusives', and 'Renangkali Granite' by Elburg et al. (2003). K-Ar ages from hornblende, feldspar and muscovite, Ar-Ar ages from muscovite,

and one U-Pb age from zircon range from c. 33.4 ± 0.2 Ma to 51.5 Ma and indicate intrusion during the Eocene to Oligocene (Sukamto, 1973; Elburg et al., 2003; van Leeuwen & Muhardjo, 2005).

2.4.2 Neogene granitoids and diorites

Granitoid bodies in the Neck region and further south in Central Sulawesi were assigned to the 'Dondo Suite', 'Dondo Batholith' or 'Dondo Super Suite' (DSS) by Kavalieris et al. (1992), van Leeuwen et al. (1994) and Elburg et al. (2003), respectively, and were considered to range in age from 12 to 0.55 Ma (van Leeuwen et al., 1994) or 9 to 1.6 Ma (Elburg et al., 2003). A group termed 'DSS Leucocratics' in the southern Neck yielded a Pliocene K-Ar age from muscovite of 3.4 ± 0.1 Ma (Elburg et al., 2003).

There was widespread K-rich granitoid and diorite magmatism during the Middle Miocene to Pliocene in Central Sulawesi (Sukamto, 1973; Sukido et al., 1993; Priadi, 1993; Priadi et al., 1994; Polvé et al., 1997; Elburg et al., 2003). A high-K suite of mafic to felsic shoshonitic and ultrapotassic rocks was described as a 'HK suite' by Priadi (1993), Priadi et al. (1994) and Elburg et al. (2003). Polvé et al. (1997) grouped these rocks into shoshonitic, alkaline potassic and ultrapotassic suites (SH, AK, UK). The youngest group of Neogene magmatic rocks is an intermediate to felsic high-K calc-alkaline suite (CAK) (Priadi, 1993; Priadi et al., 1994; Polvé et al., 1997; Elburg & Foden, 1999; Elburg et al., 2003).

The HK suite was considered to range in age from ~14 to 5 Ma (Elburg et al., 2003) or 13 to 10 Ma (Priadi, 1993; Priadi et al., 1994; Polvé et al., 1997). The CAK suite from 9 to 2 Ma (Elburg et al., 2003) or 6.5 to 0.6 Ma (Priadi, 1993; Priadi et al., 1994; Polvé et al., 1997). A low-K calc-alkaline (CA) suite (Fig. 2a) represents another group with K-Ar ages from amphibole of 19.24 ± 0.22 Ma and from plagioclase of 8.59 ± 0.07 Ma (Elburg & Foden, 1999).

Figure 2 shows a SiO_2 vs. K_2O diagram after Peccerillo & Taylor (1976) and a total alkali vs. silica (TAS) diagram after Cox et al. (1979) for a large set of analyses of the HK and CAK suites from the literature (Priadi, 1993; Priadi et al., 1994; Elburg & Foden, 1999; Elburg et al., 2003). These Neogene calc-alkaline to shoshonitic rocks were assigned to the HK or CAK suites by previous authors based on their geochemical and isotopic compositions. However, although the two suites are largely separated on the

chemical plots (Fig. 2), the SiO_2 vs. K_2O diagram of Elburg et al. (2003) shows they overlap. Furthermore, one andesite and one diorite with HK compositions were assigned to the CAK suite based on a K-Ar age of c. 2.54 Ma from the andesite (Priadi, 1993). Therefore, there are some uncertainties about the timing of different magmatic episodes.

3. Sampling and methodology

3.1 Sample collection

Metamorphic rocks and intrusive granitoids and diorites from west Central Sulawesi were the subject of this study (Fig. 3). Lithologies include metapelites and gneisses of the Palu Metamorphic Complex, gneisses from mid Central Sulawesi, Paleogene granitic stocks and sills, and Neogene granitoid and diorite intrusions. Fresh rocks with minimal alteration were sampled from outcrops or nearby float. Zircons were separated from thirty samples.

3.2 Mineral separation and preparation for geochronological analyses

Zircon extraction was carried out in the mineral separation laboratory at Royal Holloway, University of London, UK. Rocks were crushed with a jaw crusher and wet sieved with disposable nylon meshes to obtain a grain size fraction between 250-63 μm. Standard heavy liquids were used for mineral separation. Zircons were subsequently enriched using the Frantz magnetic separator, and further concentrated by hand-picking under a binocular microscope. The zircons were then mounted in epoxy resin and polished to expose mid-grain sections. Photomicrographs were taken in transmitted light to detect inclusions and cracks prior to LA-ICP-MS and SHRIMP analyses.

3.3 LA-ICP-MS

U-Th-Pb isotope analyses of 24 samples were carried out at University College London/Birkbeck College, UK using a 213 nm laser that is coupled to an Argilent 7700

quadrupole-based inductively-coupled plasma mass spectrometer (ICP-MS). A spot size of 30 μm was used. The Plešovice zircon (337.13 ± 0.37 Ma: Sláma et al., 2008) and a NIST 612 glass bead (Pearce et al., 1997) were used as standards.

GLITTER 4.4.3 (GEMOC) was used for data reduction, including calculation of uncorrected U-Th-Pb isotope ratios and age estimates at the 1σ error level. The data were corrected using the common lead correction spreadsheet by Andersen (2002), which is proposed as a ^{204}Pb common lead-independent procedure.

3.4 Secondary Ionisation Mass Spectrometry

Zircon separates from eight metamorphic and three granitic rocks from western Sulawesi were analyzed with SHRIMP II and RG at The Australian National University, Australia. The zircons were mounted in resin with the TEMORA 2 zircon standard (416.8 ± 1.0 Ma: Black et al., 2004) and polished to expose the mid-section of each grain. Photomicrographs were taken in reflected and transmitted light for all zircons to detect cracks and inclusions. Cathodoluminescence (CL) imaging was carried out on a JEOL JSM 6610A scanning electron microscope to detect internal features of the zircons (i.e. growth zonations as well as detrital/inherited cores and rim growth) and for selection of the beam spot position. Granitoid zircons were analyzed with the SHRIMP II and zircons from metamorphic samples were analyzed with the SHRIMP RG. The beam size was varied from 10 to 20 μm for rim and core analyses respectively. The TEMORA 2 U-Pb standard and SL13 uranium concentration (U = 238 ppm) standard were used for calibration. Analyses followed the procedure of Williams (1998).

3.5 U-Pb age evaluation

The ^{206}Pb-^{238}U age is given for LA-ICP-MS ages younger than 1000 Ma. Ages were considered to be concordant if the difference between the ^{206}Pb-^{238}U age and the ^{207}Pb-^{235}U age is 10% or less. The ^{207}Pb-^{206}Pb age is given for ages greater than 1000 Ma. These were considered concordant if the difference between the ^{206}Pb-^{238}U age and the ^{207}Pb-^{206}Pb age is 10% or less.

Cenozoic ages obtained by the SHRIMP analyses are ^{207}Pb common lead-corrected ^{206}Pb-^{238}U ages because of the low concentration of ^{204}Pb, ^{207}Pb and ^{208}Pb. This method

assumes each analysis is a mixture of common lead and radiogenic lead and this is unmixed from the measured ^{207}Pb-^{208}Pb ratio (e.g. Muir et al., 1996). This means that an independent age estimate from the ^{207}Pb-^{206}Pb ratio cannot be determined, so the age is determined from the ^{238}U-^{206}Pb ratio (Muir et al., 1996). SHRIMP ages greater than c. 70 Ma were corrected using the measured ^{204}Pb.

Isoplot 4.11 (Ludwig, 2003) was used to display the data on conventional Concordia (Wetherill, 1956) and Tera-Wasserburg Concordia diagrams (Tera & Wasserburg, 1972). These were used to visually assess outliers (e.g. lead loss, common lead and inheritance). Any outliers were eliminated prior to calculation of the weighted mean age (Table 1). Probability density plots were then created in Isoplot to identify different age populations. In case where several subpeaks were identified the unmix function of Sambridge & Compston (1994) in Isoplot was used to calculate a mean age for these populations (Table 1 and Supplementary Data File 1). Weighted mean ages were calculated from the youngest significant peak and usually interpreted as the most reliable estimate of the age of crystallization for each sample, unless otherwise stated. Older ages were generally interpreted as inherited. Age histograms and probability density plots were created using an R script written by I. Sevastjanova.

3.6 Geochemistry

Sample preparation and whole-rock analysis was carried out at Royal Holloway University of London, UK. Samples were crushed with a jaw crusher and milled to a fine powder in a tungsten-carbide barrel. Fusion disks and powder pellets for major and trace element analyses were measured using a PANanalytical Axios sequential X-ray fluorescence (XRF) spectrometer with a 4 kW Rh-anode X-ray tube. Reproducibility was obtained from five pellets of the same sample.

Previous geochemical analyses of the Neogene HK and CAK rocks show a very scattered distribution of samples on the SiO_2 vs. K_2O discrimination diagram (Fig. 2). Samples analyzed in this study were classified into I- type, silica-rich I-type and S-type granitoids and diorites based on the mineralogical and geochemical characteristics described by Chappell & White (1974, 2001), White & Chappell (1983) and Frost et al. (2001). These groups differ in the abundance of inherited zircon ages, which is high for S-type rocks and low for I-type and silica-rich I-type rocks. Table 2 summarizes rock

type, characteristics and geochemical data for all samples analyzed. The samples were plotted in the alumina saturation index (ASI) diagram of Frost et al. (2001) shown in Supplementary Data File 2.

S-type granitoids of this study are medium-grained granitic to granodioritic plutons or granitic dykes with biotite as the main mafic mineral (Fig. 4a, b). The samples are typically composed of quartz, K-feldspar, plagioclase and biotite, which has locally a chlorite alteration, and subordinate muscovite (Fig. 4c, d). Some of the rocks are very leucocratic and biotite is a subordinate phase only. Small metasedimentary xenoliths or biotite restites were observed at some locations, indicating a crustal-derived anatectic melt (Fig. 4b). These samples characteristically have an Fe-number between 0.68 and 0.89, a modified alkali-lime (MALI) index of 3.35 to 8.29 and an ASI index of 1.01 and 1.22 based on the indices proposed by Frost et al. (2001) as well as high SiO_2 contents (c. 69-76 wt %), low CaO contents (0.8 to 2.7 wt %) and low Ni + Cr contents (5-39 ppm). They show various effects of weak deformation, e.g. undulose extinction and formation of quartz subgrains, and bulging structures from grain boundary migration (e.g. Passchier & Trouw, 1996).

In contrast, I-type rocks in the Neck (Fig. 4e) and to the west of the Palu-Koro Fault are coarse-grained granodiorites to diorites. They are composed of quartz, K-feldspar, plagioclase, amphibole and accessory titanite and magnetite. K-feldspar forms white or pinkish pheno- to megacrysts (Fig. 4f) of variable sizes (0.5-4.0 cm). The rocks have a much higher content of mafic minerals (Fig. 4g). Some amphibole grains have remnants of clinopyroxene cores (e.g. SJH03, SJH07).

Compared to the S-type granitoids, the I-type rocks have a lower Fe-number of 0.59 to 0.61, a lower modified alkali-lime-index of -1.18 to 5.48, a lower ASI index of 0.87 to 1.00, as well as lower SiO_2 contents (c. 59-67 wt %), higher CaO contents (3.0-7.2 wt %) and higher Ni + Cr contents (97-165 ppm). The granitoids are relatively undeformed, except for some local shear zones and some deformed mafic enclaves, and undulose quartz is commonly observed in thin sections.

A few magmatic rocks were assigned to a third group, termed silica-rich I-type rocks, which contain quartz, plagioclase, K-feldspar phenocrysts, biotite and subordinate amphibole (Fig. 4h). They have an intermediate position between the S-type and I-type rocks, with respect to geochemical and mineralogical characteristics, for

example, Fe-numbers of 0.63 to 0.67, an ASI index of 1.02 to 1.03, SiO_2 contents of c. 67-70 wt %, CaO contents of 1.9 to 3.3 wt %, and Ni + Cr contents of 28 to 88 ppm.

Sample SJH11_03 shows some petrographical similarities to other rocks of the silica-rich I-type group, however, no geochemical data were obtained from this sample and therefore the sample is shown on the figures as an undefined granitoid.

4. Results of U-Th-Pb zircon dating

All data obtained by LA-ICP-MS and SHRIMP analyses are compiled in Supplementary Data Files 3 and 4, respectively. Spot numbers in the figures correspond to the analysis numbers in the data tables. U-Pb data are presented as Concordia plots (^{206}Pb – ^{238}U vs. ^{207}Pb – ^{235}U), Tera-Wasserburg Concordia plots (^{238}U – ^{206}Pb vs. ^{207}Pb – ^{206}Pb), and weighted mean diagrams in Supplementary Data File 1, and as histograms with probability density plots in Supplementary Data File 5.

Histograms were generated with bin sizes of 10 Ma for Phanerozoic ages and 50 Ma for Precambrian ages. The Phanerozoic and Precambrian ages are separated into different plots.

Possible core-rim mixing ages detected by comparison of CL imagery and photos of spot positions taken after each SHRIMP analysis were excluded from the data set (Supplementary Data File 4). Spot numbers in the tables are not continuous and represent the zircons selected for analysis. Those selected included grains of different sizes, shapes and with CL images suggesting possible core-rim age differences. A list of the samples, with their locations and calculated weighted mean ages, is shown in Table 1.

The Th/U ratio was calculated for all SHRIMP analyses and shows a broad division of low ratios (<0.1) for the majority of dark rims, which are possibly metamorphic, and high ratios for oscillatory cores and some dark and bright rims interpreted as magmatic. A low Th/U ratio is generally assumed to indicate metamorphic zircons (Ahrens, 1965; Ahrens et al., 1967). However, the ratio alone is not conclusive, because it can be affected by co-existing Th-rich minerals, such as monazite and allanite (Rubatto, 2002). Therefore, it is important to consider internal structures of the zircons, inclusions, physical parameters and the geological context of the samples (Rubatto, 2002). Monazite is present in metapelites of the PMC, whereas allanite is more common in

gneisses of the PMC (Gn50) and a few granitoid rocks in the Neck (SJH11_03) and mid Sulawesi. These co-existing accessory minerals are likely to be responsible for low Th/U ratios in zircons from these rocks.

4.1 Metamorphic rocks

4.1.1 Metapelites (Palu Metamorphic Complex)

Two metapelites were collected from the western side of the PMC in the southern Neck region (Fig. 3). SJH11_1214 combines results from two very similar rocks about 600 m apart sampled on a traverse along the road between Tawaeli and Toboli in the southern Neck (Fig. 3). The biotite schists are fine-grained with quartz veins and are composed of quartz, K-feldspar, plagioclase, biotite, garnet and an opaque phase. The zircons are colorless in transmitted light. The majority of grains are between 80-200 μm in length and predominantly euhedral prismatic to subhedral with a few subrounded grains. CL images show mainly oscillatory magmatic zoning with subordinate sector zoning, and a few grains have xenocrystic cores. No metamorphic zircon textures or rims were identified from CL imagery and the Th/U ratio is generally high (0.48 - 2.32) for the zircons analyzed. Fifteen cores and three rims from fifteen zircons were analyzed by SHRIMP. The ages show a wide Cretaceous peak (Fig. 5a) between 67.5 ± 0.9 Ma and 120.7 ± 1.7 Ma and a single age of 797.4 ± 9.9 Ma was obtained from an inherited core. The zircon shapes and age distribution suggest reworking of zircons from volcanogenic or magmatic rocks into a detrital sediment that was the schist protolith.

Sample SJH11_05 is a fine-grained schist that crops out to the east of Palu (Fig. 3). Quartz, feldspar, biotite, garnet, chlorite and magnetite are the main minerals. The zircon grains are similar to those of the schist sample SJH11_1214 with grain sizes between 90-200 μm in length. The zircons are colorless in transmitted light and predominantly euhedral to subhedral. CL images show zircons with oscillatory zoning and a few with sector zoning. The Th/U ratios are generally high (0.39 - 1.58). A few zircons have a thin or thick bright rim on CL images that could indicate a high-temperature growth during metamorphism but were not analyzed. One core with a high common lead content ($^{206}Pb_c$ = 2.94 %) yielded a SHRIMP age of 166.4 ± 2.8 Ma. Sixteen

other core and rim ages from oscillatory zoned zircons analyzed by SHRIMP define a distinct narrow peak at the Eocene/Oligocene boundary. These results are shown on a Tera-Wasserburg plot (Fig. 5b) and have a weighted mean age of 36.3 ± 0.5 Ma (MSWD = 1.4; n = 16). Oscillatory zoning or sector zoning and high Th/U ratios are interpreted to indicate that zircons have a magmatic origin and were reworked into a sediment later metamorphosed to a schist.

4.1.2 Gneisses (Palu Metamorphic Complex)

Gneisses from the eastern part of the PMC (Fig. 3) in the southern Neck are biotite gneisses (Gn46, Gn50) and biotite-amphibole gneisses (Gn48, Gn49). The former are composed of quartz, plagioclase, K-feldspar, biotite ± garnet ± allanite and an opaque phase. Biotite-amphibole gneisses include quartz, plagioclase, K-feldspar, biotite, amphibole, titanite and an opaque phase. The gneisses are foliated, with microfolds at a cm-scale. The majority of zircons from these samples are euhedral, pinkish in transmitted light and between 100 and 250 μm in length.

Twenty-four zircon rims and two cores were analyzed by SHRIMP from sample Gn46. Most of the rims are dark with variable U (216 - 16353 ppm) and Th contents (4 - 2358 ppm). Some bright rims have rather low U (135 - 518 ppm) and Th contents (8 - 52 ppm). The Th/U ratios from the dark and bright rims are generally low (0.01 to 0.4). The two ages obtained from cores are 135.1 ± 4.9 Ma and 3.8 ± 0.07 Ma. The two grains analyzed have very similar patchy internal structures, and the former grain yielded two ages from a thick dark rim and a thin dark outermost rim of 3.7 ± 0.1 Ma and 3.9 ± 0.1 Ma respectively. Therefore, the core age of c. 3.8 Ma is interpreted as reset. One analysis of a dark rim from a different grain gave an age of 61.5 ± 3.7 Ma. All other ages obtained from dark and bright rims range from 3.5 ± 0.1 Ma to 4.2 ± 0.2 Ma, after one analysis of 6.1 ± 0.5 Ma was excluded due to a high common lead content ($^{206}Pb_c$ = 24.7 %), and yielded a weighted mean age of 3.59 ± 0.04 Ma (MSWD = 1.5; n = 20) which is interpreted as metamorphic.

U-Pb SHRIMP dating of twelve zircons from sample Gn48 included three core and eleven rim analyses. Two oscillatory zoned grains have high Th/U ratios of 0.87 and 1.29, and core ages of 186.1 ± 3.3 Ma and 222.1 ± 4.0 Ma respectively. A third oscillatory zoned core with patchy dark zones yielded an age of 140.0 ± 2.7 Ma and has a dark rim

with an age of 3.6 ± 0.2 Ma. Both core and rim analyses have low Th/U ratios of 0.06 and 0.01 respectively. Analyses of dark rims from other grains gave Triassic (215.3 ± 3.3 Ma), Jurassic (189.6 ± 2.0 Ma), Cretaceous (90.2 ± 1.6 Ma; 121.1 ± 2.8 Ma) and Eocene (40.8 ± 1.4 Ma) ages with Th/U ratios between 0.08 and 1.58, and six Late Miocene to Pliocene ages with low Th/U ratios between 0.01 and 0.08 and relatively low U (108 - 599 ppm) and Th contents (1-10 ppm). A mean age of 3.67 ± 0.16 Ma (MSWD = 0.72) was calculated from five of these six Neogene rim analyses. One age of 6.2 ± 0.4 Ma was excluded due to a high common lead content ($^{206}Pb_c$ = 20.4 %).

Seven cores and nine rims were analyzed by SHRIMP from fourteen zircons of sample Gn49. All of them have relatively high Th/U ratios (0.07 - 1.09). Uranium and thorium contents of cores are generally low (U = 113 - 1327 ppm; Th = 73 - 475 ppm), whereas they are high for rims (U = 735 - 2281 ppm; Th = 58 - 1548 ppm). Ages of cores with oscillatory to partly convolute disturbed zoning are mainly Triassic (211.6 ± 2.5 Ma to 223.8 ± 2.6 Ma), with a few Jurassic (171.5 ± 2.4 Ma; 194.8 ± 2.7 Ma) and Cretaceous (106.8 ± 2.8 Ma) ages. A rim age of 141.5 ± 2.5 Ma was obtained from the grain with a convolute disturbed core age of 171.5 ± 2.4 Ma. Analyses of other grains with patchy dark rims or oscillatory zoned rims have a similar age span of Triassic to Cretaceous (109.0 ± 2.0 Ma to 214.0 ± 2.7 Ma) with two Eocene ages (41.0 ± 0.4 Ma; 44.9 ± 1.5 Ma).

Five zircon cores and fourteen rims were analyzed by SHRIMP from eighteen zircons of sample Gn50. Allanite was observed in a thin section of this sample and Th has probably partitioned into allanite, resulting in low Th/U ratios in the zircons. Oscillatory zoned cores are Triassic to Jurassic (166.5 ± 2.5 Ma to 232.9 ± 6.0 Ma) with high Th/U ratios (0.65 - 1.54). One core with irregular patchy internal structures has a relatively low Th/U ratio of 0.21 and yielded a Late Eocene age of 37.3 ± 1.0 Ma. The core with an age of 166.5 ± 2.5 Ma has a thin dark and outermost bright rim which has a low Th/U ratio of 0.18 and an age of 51.6 ± 3.8 Ma. Other analyses of dark and outermost light rims have low Th/U ratios of 0.01 to 0.13 with moderate U (107 - 1628 ppm) and low Th contents (4 - 79 ppm). These rims yielded one Cretaceous age (78.7 ± 1.4 Ma), another Eocene age (54.5 ± 1.7 Ma), and a majority of Late Miocene to Pliocene ages (9.5 ± 0.2 Ma to 3.5 ± 0.1 Ma). A few Late Miocene or Pliocene ages from rims with some common lead ($^{206}Pb_c$ = 1.7 - 4.6 %) were disregarded for the calculation of the weighted mean age of 3.63 ± 0.07 Ma (MSWD = 0.94; n = 7).

The protoliths of the PMC gneisses are suggested to be sediments or granitoids of Mesozoic age. The oscillatory zoned grains and cores resemble magmatic zircons. No ages older than Mesozoic were obtained (Fig. 6a, b). Scattered Jurassic, Cretaceous and Paleogene ages from oscillatory cores with localized patchy internal structures and dark rims are either affected by lead loss or possibly a later metamorphic overprint. Analyses of irregular dark zircon rims with partly light outermost rims with low Th/U ratios record a very young metamorphic overprint at c. 3.6 Ma (Fig. 6c, d). A very small number of Late Miocene ages were not included in the mean age calculations, because they were from spots where the beam intersected multiple zones, they scatter off the Concordia, or have a high common lead content ($^{206}Pb_c$ = 24.7 %, Gn46; $^{206}Pb_c$ = 20.44 %, Gn48). Single analyses between 20-40 Ma are interpreted as mixed ages due to intersection of the beam with cores and rims.

4.1.3 Gneisses (mid Central Sulawesi)

Gneisses from mid Central Sulawesi were sampled south of the Palolo Basin and east of the Besoa Basin (Fig. 3). The rocks are weakly deformed (amphibole-) biotite gneisses (SJH28, SJH11_99), and a garnet-bearing biotite gneiss (SJH11_113).

Seventy-four zircons from sample SJH28 were analyzed by LA-ICP-MS. The grains are c. 60-250 µm in length, prismatic and colorless in transmitted light. The Concordia plot shows that some zircons have experienced lead loss; there is an upper intercept at 1380 ± 32 Ma and a poorly defined lower intercept of Paleozoic or Mesozoic age. The concordant zircons form a dominant Mesoproterozoic population with a weighted mean age of 1336.1 ± 9.5 Ma (MSWD = 0.7; n = 37), which is interpreted as a magmatic age. These Proterozoic zircons were reworked into a detrital sediment that was melted during the Paleozoic or Mesozoic.

Sample SJH11_113 was analyzed by LA-ICP-MS and SHRIMP. The grains are between 80 and 200 µm in length and include euhedral, subhedral, and subrounded grains with prismatic and bipyramidal grain shapes, as well as a few subangular fragments. The zircons show oscillatory zoning or have xenocrystic cores. Some have thick dark or thin bright rims, or convolute disturbed oscillatory zoned rims. Seventy-one zircons from sample SJH11_113 were analyzed by LA-ICP-MS. They contain zircons with main age populations that are Proterozoic (peak at 1.4-1.5 Ga) and Triassic to

Jurassic (163 ± 2 Ma to 251 ± 3 Ma), and several scattered Cambrian, Ordovician, Devonian, Carboniferous and Permian ages (Fig. 7). The conventional Concordia diagram shows core and rim analyses plot along a Discordia line similar to sample SJH28. An upper intercept age is 1517 ± 49 Ma, but if the oldest discordant zircon age of 2.1 Ga is excluded an upper intercept age of 1414 ± 25 Ma is obtained. A weighted mean age of 1417 ± 11 Ma (MSWD = 0.87; n = 12) was calculated from the concordant analyses and is interpreted as a magmatic crystallization age. A lower Concordia intercept at 220 ± 16 Ma includes three age populations with weighted mean ages of 199. 3 ± 2.0 Ma (MSWD = 0.67; n = 5), 212.7 ± 2.8 Ma (MSWD = 4.1; n =15) and 234.7 ± 2.0 Ma (MSWD = 2.6; n = 27) which are interpreted as magmatic episodes in the Triassic, based on oscillatory zoning on CL images. The wide age range, including Proterozoic, Paleozoic and Mesozoic zircons, indicates reworking of grains of different ages into a detrital sediment that was the gneiss protolith.

SHRIMP analyses were obtained from ten other zircons from sample SJH11_113 which yielded twelve core and seven rim ages. Proterozoic inherited grains (1269.8 ± 17.3 Ma to 2427.4 ± 22.4 Ma) have rounded xenocrystic cores on CL images and oscillatory zoned rims with ages of 1082.8 ± 14.3 Ma and 1204.7 ± 12.9 Ma, or disturbed oscillatory zoned rims with ages of 9.4 ± 0.3 Ma and 559.9 ± 5.8 Ma. Zircons of Devonian age (364.3 ± 4.4 Ma to 369.6 ± 4.3 Ma) are xenocrystic or oscillatory zoned. One xenocrystic core with an age of 369.6 ± 4.3 Ma has a thick dark rim with a low Th/U ratio of 0.03 and an age of 83.8 ± 1.3 Ma. Another xenocrystic core with an age of 368.7 ± 7.7 Ma is embayed and has a bright rim with an age of 4.6 ± 0.2 Ma. Several Triassic ages were obtained from oscillatory zoned grains (206.8 ± 4.6 Ma to 239.3 ± 3.4 Ma). One of them has a disturbed oscillatory zoned rim with an age of 11.1 ± 0.4 Ma. All convolute disturbed oscillatory zoned rims analyzed give scattered Middle Miocene to Pliocene ages (4.6 ± 0.2 Ma to 11.1 ± 0.4 Ma). These rims have high common lead contents ($^{206}Pb_c$ = 8.3 - 21.3 %) and no weighted mean age could be calculated. The Th/U ratios are very low (0.01 to 0.03) and may indicate a metamorphic origin. However, some intact oscillatory zoning suggests a magmatic origin for some rims, and the low Th/U ratio may be the result from partitioning of Th into monazite.

Zircons from sample SJH11_99 were analyzed by LA-ICP-MS (56 grains) and SHRIMP (19 grains). They are euhedral to subhedral with a few subrounded and subangular grains and a predominantly large grain size from 100 to 300 μm in length.

SHRIMP ages from nine zircon cores and seventeen rims display a strong Triassic peak at c. 230 Ma and a possible Jurassic peak at c. 165 Ma (Fig. 8 and Supplementary Data File 1). Other scattered ages are probably affected by lead loss, indicated by LA-ICP-MS analyses plotting off the Concordia curve. The Triassic grains have mostly magmatic oscillatory zoning. One grain with a Triassic core age of 225.2 ± 4.5 Ma has a thick dark convolute disturbed rim with an age of 158.4 ± 3.0 Ma. Analyses from other cores with patchy structures, or bright or dark rims yielded Jurassic ages from 146.4 ± 3.2 Ma to 171.7 ± 2.9 Ma, and Cretaceous ages from 104.7 ± 2.6 Ma to 136.7 ± 2.5 Ma. A relict core with an age of 184.1 ± 3.6 Ma has a thick dark rim with an age of 3.2 ± 0.4 Ma (Fig. 8). Other analyses from thick dark rims and/or thin light outermost rims have low Th/U ratios (0.02 - 0.27) with moderate U (23 - 780 ppm) and Th contents (2 - 200 ppm) and yielded Late Miocene to Pliocene (3.1 ± 0.3 Ma - 9.7 ± 2.4 Ma) ages with a mean age of 3.12 ± 0.32 Ma (MSWD = 0.10; n = 5). The internal structures of grains and the low Th/U ratios indicate a metamorphic origin (Fig. 8).

4.2 Granitoids and diorites

4.2.1 Paleogene rocks

A granodiorite (SJH06) from west of Palu valley (Fig. 3) is a Paleogene intrusive stock. It consists of quartz, plagioclase and K-feldspar with sericite alteration, biotite, chlorite, and subordinate muscovite, epidote, garnet and ilmenite. The zircons are mainly euhedral to subhedral, 60-200 μm in length, and show oscillatory zoning on CL images and a few grains with obvious cores.

LA-ICP-MS analyses of 58 grains yielded 28 concordant ages Devonian, Triassic, Cretaceous, and Paleocene ages from cores. Most concordant ages are from grains with oscillatory zoning and are Late Eocene to Early Oligocene. Their weighted mean age of 35.16 ± 0.65 Ma (MSWD = 2.1; n = 18) is considered to be magmatic.

This interpretation was supported by SHRIMP analyses of thirteen cores and nine rims from twenty zircons. Five rim analyses were excluded due a possible metamict character of the zircon or matrix-dependent secondary ionization effects of the beam (White & Ireland, 2012). They are mixed ages from different zones with high U contents (1410 - 6390 ppm), which are correlated with an increase in age (c. 37 to 41 Ma). Th/U

ratios from all accepted analyses are relatively high (0.43 to 1.55) and indicate a magmatic origin for the oscillatory zoned zircons. Two inherited cores have ages of 52.7 ± 1.3 Ma and 198.9 ± 2.9 Ma with oscillatory zoned rims with ages of 34.5 ± 0.7 Ma and 34.3 ± 1.0 Ma respectively. Thirteen other core and rim ages were obtained from oscillatory zoned grains which have similar Late Eocene to Oligocene ages and yield a mean age of 35.1 ± 0.5 Ma (MSWD = 0.6; n = 15). This age is considered to be magmatic based on the oscillatory zoning and the high Th/U ratios.

A small granitic sill (SJH11_10) to the northeast of Palu (Fig. 3) cuts dioritic rocks that are associated with intermediate to basaltic rocks of Middle Eocene to Middle Oligocene age based on K-Ar analyses (Polvé et al., 1997; van Leeuwen & Muhardjo, 2005). LA-ICP-MS ages of 44 zircons with 12 concordant grains from SJH11_10 are similar to those from the granodiorite stock (SJH06). Zircons have Triassic (210.0 ± 3.0 Ma), Cretaceous (127.0 ± 2.0 Ma) and Late Eocene (31.8 ± 0.6 Ma to 39.0 ± 1.0 Ma) ages. A weighted mean age of 33.1 ± 1.1 Ma (MSWD = 1.7) was calculated from the six Eocene ages and interpreted as the crystallization age of the granite. The mean ages calculated for sample SJH06 and SJH11_10 confirm a Late Eocene to Early Oligocene age for the Paleogene granitic stocks and sills.

4.2.2 Neogene rocks

Neogene magmatic rocks analyzed in this study are granites, granodiorites and diorites (Table 2) based on the total alkali vs. silica (TAS) diagram (Cox et al., 1979) and the R1-R2 plot (de la Roche et al., 1980). The diorites are classified as quartz-monzodiorites in the CIPW normative QAPF diagram (Streckeisen, 1974).

4.2.3 Neogene felsic granitoid intrusions (S-type)

Granitic dykes cross-cut schists from the PMC (SJH01) and ultrabasic rocks in mid Sulawesi (SJH11_103). Their thickness varies from a few tens of centimeters to several meters. Contacts are locally irregular and faulted, indicating post-emplacement deformation. The dykes are heavily fractured with subhorizontal and subvertical sets of joints.

Zircons from a dyke (SJH01) from the Tawaeli-Toboli Neck road traverse (Fig. 3) were analyzed by LA-ICP-MS and SHRIMP. The zircons are predominantly orange colored in transmitted light, and euhedral with subordinate subhedral to subrounded and subangular grains. The grains are between c. 60 and 300 µm in length. Many show oscillatory zoned cores on CL images with high Th/U ratios of 0.53 to 1.68. Some grains have irregular dark or bright rims (Fig. 9) with variable Th/U ratios (0.02 - 0.40).

Twenty-six of seventy-three LA-ICP-MS analyses from seventy grains are concordant, with Triassic (200.0 ± 3.0 Ma to 238.0 ± 3.0 Ma), Jurassic (163.0 ± 2.0 Ma to 197.0 ± 3.0 Ma) and Cretaceous (129.0 ± 2.0 Ma to 136.0 ± 2.0 Ma) ages. The youngest Cenozoic zircons analyzed have scattered Late Miocene to Pliocene ages (3.2 ± 0.1 Ma to 9.6 ± 0.3 Ma) and no weighted mean age could be calculated.

SHRIMP analyses were obtained from twelve other zircons from sample SJH01 which yielded twelve core and nine rim ages. The cores have Triassic (212.5 ± 2.8 Ma - 224.2 ± 2.5 Ma), Jurassic (165.4 ± 3.8 Ma - 188.5 ± 6.1 Ma), and Cretaceous (112.0 ± 1.6 Ma - 140.3 ± 4.0 Ma) ages. Irregular dark and bright rims analyzed from oscillatory zoned grains with Triassic, Jurassic or Cretaceous core ages, and a few other grains, yielded Late Miocene to Pliocene ages (2.9 ± 0.3 Ma - 8.3 ± 0.8 Ma) with high common lead contents ($^{206}Pb_c$ = c. 10 - 50 %). A mean age of 3.14 ± 0.18 Ma (MSWD = 1.08; n = 5) was calculated from ages between 2.9 ± 0.3 Ma and 3.2 ± 0.1 Ma (Fig. 9). The Mesozoic ages are from zircons with oscillatory zoning and indicate reworking of magmatic rocks into a detrital sediment. The weighted mean age calculated from the rim ages is interpreted as magmatic crystallization age of the granitic dyke (SJH01). A Pliocene metamorphic event based on zircon ages from gneisses (Gn46, Gn48, Gn50, SJH11_99) described earlier would explain the variable Th/U ratios of zircon rims from the granite.

A granitic dyke (SJH11_103) cross-cutting peridotites south of the Palolo Basin in mid Central Sulawesi (Fig. 3) was analyzed by LA-ICP-MS and SHRIMP. Zircons are mainly euhedral to subhedral and subordinately subangular, c. 60-200 µm in length, and colorless to orange in transmitted light. CL images show oscillatory zoning, or bright, round xenocrystic cores with dark rims and/or oscillatory zoned rims. The rims have predominantly high Th/U ratios of 0.13 - 1.01 (two have low ratios of 0.02 and 0.05), indicating a melt-derivation. Uranium (49 - 6216 ppm) and thorium contents (23 - 6179 ppm) of the dark rims vary widely.

Fifty-two LA-ICP-MS analyses with thirty-eight concordant ages yielded Proterozoic, Paleocene, Eocene, Early Miocene, and Pliocene ages. Early Pliocene ages range from 4.1 ± 0.1 to 4.5 ± 0.2 Ma and form a minor peak at 4.19 ± 0.13 Ma (MSWD = 1.09; n = 4). Many Late Pliocene ages were obtained which range from 2.2 ± 0.1 Ma to 3.2 ± 0.1 Ma and give a mean age of 2.53 ± 0.10 Ma (MSWD = 3.7; n = 18).

Five xenocrystic cores analyzed by SHRIMP yielded Proterozoic, Carboniferous, Jurassic, Cretaceous and Eocene ages. Sixteen analyses of wide oscillatory zoned and dark rims yielded Neogene ages (2.3 ± 0.8 Ma to 5.5 ± 0.2 Ma). Some ages define a minor peak at c. 4.4 Ma. The majority yield a Late Pliocene weighted mean age of 2.95 ± 0.07 Ma (MSWD = 1.14; n = 12) on a Tera-Wasserburg Concordia plot (Fig. 10). The xenocrystic cores are interpreted as detrital. The Pliocene ages from oscillatory zoned rims are considered to represent magmatic crystallization ages, similar to sample SJH01. Coeval dark rims are possibly related to metamorphism identified from zircon ages from gneisses (Gn46, Gn48, Gn50, SJH11_99).

Zircons from several other granitoids were analyzed by LA-ICP-MS. Samples included granitic dykes in the metamorphic rocks from east of Palu valley (SJH18, SJH11_60; Fig. 3), granites and granodiorites from both sides of the Palu-Koro Fault to the south of Gimpu (SJH11_71, SJH11_75; Fig. 3), a granite from the southeast of the Palolo Basin (SJH11_107; Fig. 3), as well as a granodioritic intrusion in the high mountain range between the Besoa and the Bada Basins (SJH11_121/122; Fig. 3). The zircons are euhedral, subhedral or subrounded with prismatic or bipyramidal shapes, c. 60-300 μm in length, and orange or colorless in transmitted light. Ages from 230 concordant grains display a strong Late Miocene to Pliocene peak (2.1 ± 0.3 Ma - 8.5 ± 0.4 Ma), a wide Mesozoic to Cenozoic peak (11.7 ± 0.4 Ma - 232.0 ± 3.0 Ma), and scattered ages in the Permian, Carboniferous, Silurian, Ordovician and Cambrian. Four Proterozoic ages (581 Ma, 824 Ma, 840 Ma, and 1.5 Ga) and one Archean age (3.1 Ga) were obtained.

Several scattered Middle Miocene to Early Pliocene ages are probably affected by lead loss and were excluded from the weighted mean age calculation. The mean ages calculated are summarized in Fig. 11a and Table 1. Age ranges determined for each sample are shown in Fig. 11b. Weighted mean age diagrams with probability density plots are shown in Supplementary Data File 1.

Ages obtained from sample SJH18 range from 3.7 ± 0.2 Ma to 4.7 ± 0.3 Ma and form a single wide peak in the probability density plot. A weighted mean age of 4.07 ± 0.08 Ma (MSWD = 2.0; n = 21) was calculated. Sample SJH11_60 has a range of ages between 3.9 ± 0.1 Ma and 5.1 ± 0.3 Ma, after two youngest ages obtained, of 3.3 ± 0.1 Ma and 3.5 ± 0.1 Ma, are interpreted to be affected by lead loss. The plot shows a wide peak, including a younger subpeak with a weighted mean age of 4.12 ± 0.10 Ma (MSWD = 1.4; n = 10) and a slightly older subpeak with a weighted mean age of 4.63 ± 0.15 Ma (MSWD = 1.5; n = 6). Sample SJH11_71 has a range in age from 3.1 ± 0.1 Ma to 4.4 ± 0.1 Ma. The probability density plot shows a wide peak, including a younger subpeak with a weighted mean age of 3.78 ± 0.07 Ma (MSWD = 2.9; n = 25) and the slightly older subpeak with a weighted mean age of 4.29 ± 0.10 Ma (MSWD = 1.6; n = 9). Sample SJH11_75 has a range of ages from 2.8 ± 0.1 Ma to 3.8 ± 0.1 Ma. The probability density plot shows a bimodal age distribution, including a younger peak with a weighted mean age of 2.92 ± 0.08 Ma (MSWD = 0.76; n = 8) and a slightly older peak with a weighted mean age of 3.61 ± 0.13 Ma (MSWD = 2.4; n = 8). Sample SJH11_107 yielded ages ranging from 2.6 ± 0.1 Ma to 4.6 ± 0.1 Ma, after the youngest age obtained, of 2.1 ± 0.3 Ma, is interpreted as affected by lead loss. The probability density plot shows one subpeak with a weighted mean age of 3.11 ± 0.10 Ma (MSWD = 0.49; n = 5), a slightly younger subpeak at c. 2.7 Ma, as well as several small older subpeaks with the oldest at c. 4.5 Ma. Sample SJH11_121/122 shows a range of ages between 2.6 ± 0.1 Ma and 4.3 ± 0.1 Ma in the probability density plot. The ages form a younger peak with a weighted mean age of 3.05 ± 0.12 Ma (MSWD = 4.6; n = 17) and a smaller older peak with a weighted mean age of 4.13 ± 0.16 Ma (MSWD = 2.3; n = 6).

4.2.4 Neogene intermediate granitoid and diorite intrusions (I-type and silica-rich I-type)

Eleven granitoid and diorite intrusions (Fig. 3) were sampled from the west side of the Neck (from north to south: SJH11_36, SJH11_45, SJH11_48, SJH05, SJH03, SJH11_03), the mountains west of the Palu-Koro Fault (SJH07, SJH08), the large 'Kambuno granite' intrusion near Masamba northwest of Bone Bay (SJH11_125), and from the Mamasa/Polewali intrusions in southern West Sulawesi (SRH42, SRH49).

The zircons separated from these intrusions are euhedral prismatic with large grains from 100 to a maximum of 550 μm in length and a deep orange color in transmitted light. Some lead loss is indicated by the Concordia plots (Supplementary Data File 1). Eight concordant grains have Devonian, Permo-Triassic, Jurassic and Cretaceous ages.

The Late Miocene to Pliocene ages include some outliers that were excluded from the weighted mean age calculations. All mean ages calculated for the I-type and silica-rich I-type granitoids and diorites are summarized in Fig. 11a and Table 1. Age ranges determined for each sample are shown in Fig. 11b. Probability density plots and weighted mean age diagrams for the youngest peak are displayed in the Supplementary Data File 1.

Sample SJH11_36 yielded ages from 3.6 ± 0.2 Ma and 6.2 ± 0.2 Ma. A weighted mean age of 5.07 ± 0.10 Ma (MSWD = 2.4; n = 45) was calculated from a wide peak on the probability density plot. Sample SJH11_45 has a range of ages from 4.3 ± 0.2 Ma to 8.1 ± 0.3 Ma. The probability density plot shows a wide peak which has two subpeaks. A weighted mean age of 5.08 ± 0.09 Ma (MSWD = 1.8; n = 17) was calculated for the younger subpeak. The second slightly older subpeak yielded a weighted mean age of 5.55 ± 0.07 Ma (MSWD = 0.73; n = 16). Ages from sample SJH11_48 range from 6.4 ± 0.2 Ma to 8.6 ± 0.2 Ma. The probability density plot shows a narrow peak with a weighted mean age of 7.36 ± 0.09 Ma (MSWD = 3.6; n = 26). Sample SJH05 includes ages ranging from 4.5 ± 0.3 Ma to 7.2 ± 0.1 Ma. The probability density plot shows a wide peak with a narrow subpeak with a weighted mean of 6.08 ± 0.08 Ma (MSWD = 0.91; n = 10), and two slightly older and younger subpeaks. The small younger subpeak is at c. 5.6 Ma and the older subpeak has a weighted mean age of 6.71 ± 0.16 Ma (MSWD = 0.20; n = 5). Ages obtained from sample SJH03 range from 6.0 ± 0.2 Ma to 8.5 ± 0.3 Ma. The probability density plot has a wide peak with a weighted mean age of 6.97 ± 0.10 Ma (MSWD = 9.7; n = 67). Sample SJH07 yielded ages ranging from 6.3 ±0.2 Ma to 8.6 ± 0.3 Ma, and one concordant outlier of 10.5 ± 0.4 Ma. A wide peak on the probability density plot has a weighted mean age of 7.15 ± 0.13 Ma (MSWD = 6.2; n = 59). Ages obtained from sample SJH08 range from 5.4 ± 0.2 Ma to 8.4 ± 0.2 Ma. One age of 9.1 ± 0.2 Ma falls off the Concordia, and was therefore excluded. The probability density plot shows a wide peak which produced a weighted mean age of 6.74 ± 0.07 Ma (MSWD = 5.0; n =46). Ages from sample SJH11_125 range from 5.7 ± 0.1 Ma to 8.3 ± 0.2 Ma, after the youngest

ages, of 5.2 ± 0.1 Ma to 5.5 ± 0.1 Ma, are interpreted as affected by lead loss. The probability density plot shows a wide peak which includes two age populations. The younger subpeak has a weighted mean age of 6.21 ± 0.08 Ma (MSWD = 2.7; n = 30); the slightly older subpeak has a weighted mean age of 6.91 ± 0.08 Ma (MSWD = 1.4; n = 21). The main age population in sample SRH42 ranges from 5.5 ± 0.3 Ma to 7.9 ± 0.3 Ma, and there is one outlier of 13.7 ± 0.4 Ma. One age of 16.2 ± 0.9 Ma has a high common lead content and was excluded. The probability density plot has a wide peak which consists of two age populations. They have weighted mean ages of 6.41 ± 0.09 Ma (MSWD = 0.82; n = 25) and 7.12 ± 0.08 Ma (MSWD = 0.54; n =25). Ages obtained from sample SRH49 range from 4.1 ± 0.2 Ma to 6.1 ± 0.3 Ma. The probability density plot shows a single peak which has a weighted mean age of 5.32 ± 0.11 Ma (MSWD = 2.7; n = 21).

Sample SJH11_03 includes two ages of 3.5 ± 0.1 Ma and 3.7 ± 0.1 Ma interpreted to be affected by lead loss, and a small number of older ages (5.8 ± 0.3 Ma - 8.4 ± 0.3 Ma) which mostly have a high common lead content and may be affected by partial Pb loss, as indicated by the Concordia and Tera-Wasserburg Concordia diagrams (Supplementary Data File 1). After excluding these, SJH11_03 has a range of ages from 3.9 ± 0.1 Ma to 5.3 ± 0.4 Ma. The probability density plot shows a younger subpeak with a weighted mean age of 4.06 ± 0.05 Ma (MSWD = 0.85; n = 15) and an older subpeak with a weighted mean age of 4.57 ± 0.10 Ma (MSWD = 4.0; n = 21).

5. Discussion

5.1 Origin and protoliths: west Central Sulawesi

Protoliths of metamorphic rocks of west Central Sulawesi were pelitic sediments based on zircon age populations interpreted as detrital, or metagranitoids with inherited zircons. Main peaks identified from histograms and probability density plots, and data points clustering on Concordia diagrams, are Mesoproterozoic (c. 1.3 - 1.5 Ga), Mesozoic from the Triassic to the Cretaceous (c. 80 - 250 Ma) with Jurassic (c. 165 Ma), and Paleogene subpeaks (Fig. 12). There are also Neoproterozoic, Cambrian, Ordovician, Silurian, Devonian, Carboniferous, and Permian ages. Concordia plots of LA-ICP-MS and SHRIMP analyses show scattered Late Miocene to Pliocene ages that are affected by inheritance, lead loss and common lead.

West Central Sulawesi was previously interpreted to be part of an East Java-West Sulawesi block (Hall et al., 2009; Hall, 2011, 2012). Reconstructions positioned this block in a relatively western position in the Australian continental margin when rifting started in the Late Jurassic, before accretion to the southeastern promontory of Sundaland in the Late Cretaceous (Hall et al., 2009; Metcalfe, 2011; Hall, 2012). This was based on the presence of Archean to Cambrian zircons reported from East Java and Western Sulawesi, and on geochemical evidence for Australian-origin crust beneath western Sulawesi (Elburg et al., 2003).

5.1.1 Inherited zircons

Zircons found in the southern part of East Java indicate continental crust beneath the island with a west Australian origin (Smyth et al., 2007, 2008; Hall et al., 2009). Comparisons of the East Java zircon data (Smith et al., 2008) show Archean zircons at c. 2.8-3.6 Ga similar in age to the Pilbara craton, and a peak at c. 2.7 Ga, resembling ages from the Yilgarn craton (Sircombe & Freeman, 1999; Neumann & Fraser, 2007). Archean zircons were also obtained from Western Sulawesi (van Leeuwen et al., 2007) and were thought likely to be similar to those from East Java although only a small number of ages were reported.

However, the histogram including all inherited ages from metamorphic and S-type granitoids from this study (Fig. 12), shows that within a relatively large number of Precambrian ages (n = 87), only one Archean age was acquired (Fig. 12). This is very different from East Java, where the proportion of Archean ages is much greater (Smyth et al., 2008). The dominant Mesoproterozoic age population (n = 53) is more similar to ages from rocks from the Bird's Head of New Guinea (Gunawan et al., 2012).

Many Phanerozoic ages were obtained from the Sulawesi samples in this study and there is a prominent Triassic peak, which is present in almost all samples. This population is absent in East Java and in Western Australia but is typical of the Bird's Head region of New Guinea. The Mesozoic and Paleozoic zircon age populations show great similarities to those of the Tipuma Formation in the Bird's Head, New Guinea (Gunawan et al., 2012; Gunawan, 2013). The Tipuma Formation has Proterozoic ages with main peaks at 1.0 Ga, 1.3-1.6 Ga and 1.8 Ga, Carboniferous ages, and a strong Permo-Triassic peak. Permo-Triassic and Proterozoic ages are also common in zircons

from Borneo and the Malay Peninsula. However, they have a significantly smaller peak at 1.5 Ga and prominent peaks at 1.0-1.2 Ga and 500 Ma, which is rarely present in the samples from the Bird's Head (Hall & Sevastjanova, 2012; van Hattum et al., 2013). Devonian and Carboniferous ages are rare to absent in the Malay Peninsula (Sevastjanova et al., 2011).

We consider the zircon age data obtained from this study are best explained by interpreting NW Sulawesi to have been positioned east of the Argoland terrane, and to have formed part of the Inner Banda Embayment block. This would have been close to the Australian continent and the Bird's Head from which it would have received an important contribution of detrital zircons (Fig. 13). This requires no significant modification of the reconstructions of Hall (2012) but simply a reassignment of NW Sulawesi to the Inner Banda fragment rather than the East Java-West Sulawesi fragment and a small adjustment of fragment boundaries (Fig. 13). The Late Jurassic to Late Eocene tectonic evolution of NW Sulawesi, including source regions, is summarized in Fig. 14.

So far, no Jurassic rocks have been found in western Sulawesi. The Jurassic zircon ages may be related to rifting of the Inner Banda block (NW Sulawesi) from the Australian margin of Gondwana. The Cretaceous zircons, and possibly also some or all of the Jurassic zircons, are interpreted as detrital grains derived from Borneo. Their ages resemble those of zircons from the Pinoh Metamorphic Group and the Schwaner intrusions of west Borneo, which have distinctive Cretaceous peaks at c. 80-85 Ma, 110-120 Ma and 130 Ma (Davies, 2013; Davies et al., 2014). Cretaceous metamorphism in Borneo has been related to the emplacement of the Schwaner intrusive bodies (Davies, 2013; Davies et al., 2014). Jurassic granitoids have been reported from the South Schwaner region (Haile et al., 1977) and confirmed by dating of zircons from that region (Davies, 2013; van Hattum et al., 2013).

The schists from the PMC have previously been assumed to have been part of an Australian-derived terrane, which had a Paleozoic or Lower Mesozoic metamorphic basement partly overprinted by Late Mesozoic metamorphism associated with subduction and collision (Sukamto, 1973; Sopaheluwakan et al., 1995; Parkinson et al., 1998). The presence of detrital Cretaceous zircons in the metapelite SJH11_1214 analyzed shows this cannot be the case for some of the metamorphic rocks. Zircon age populations from the schists from the PMC with ages between 80 to 120 Ma resemble

those from Borneo and suggest that volcanogenic and plutonic rocks of Sundaland were an important source region for the sediments that were the protoliths of some of the metamorphosed rocks in the Neck of Sulawesi. This supports a previously suggested Sundaland parentage for some of the rocks of the PMC (van Leeuwen & Muhardjo, 2005). The widespread Latimojong Formation in mid Central Sulawesi includes sedimentary to low-grade metasedimentary rocks which in some areas contain Late Cretaceous zircons (van Leeuwen & Muhardjo, 2005). These could be the unmetamorphosed and low grade equivalents of the highly deformed schists of the PMC.

Late Eocene to Early Oligocene zircons confirm that some protoliths of the PMC are much younger than previously supposed. One schist sample from the PMC (SJH11_05) contains zircons interpreted as detrital with Late Eocene to Early Oligocene ages. Zircons from two Paleogene granites from east and west of Palu have Late Eocene to Early Oligocene ages, interpreted as the age of granite emplacement. Several granitic and metamorphic samples analyzed in this study contain zircons with concordant Eocene ages. They are interpreted to record a magmatic event, possibly related to rifting and extension in the Makassar Straits now separating western Sulawesi from east Borneo. Reworking of zircons into a detrital and/or a volcanogenic protolith is proposed for the schist.

5.2 Neogene magmatism

Granitoids in Western Sulawesi were previously grouped into a HK suite (14-5 Ma) and a CAK suite (9-2 Ma) by Elburg et al. (2003) with ages based on K-Ar dating. Several granitoid intrusions in the area analyzed in this study are chemically similar to the CAK suite (SiO_2 content >60%). LA-ICP-MS and SHRIMP analyses of zircons show two magmatic episodes, which are Late Miocene to Early Pliocene, and Early to Late Pliocene (Fig. 11a, b).

The U-Pb ages from this study define two different magmatic episodes with shorter intervals than those based on the K-Ar ages reported for the CAK suite. One magmatic phase at c. 8.5-4 Ma produced intrusive bodies along the western side of the Neck and along the west side of the Palu-Koro Fault. The variations in the calculated mean ages (c. 7.5-5 Ma; Fig. 11a), as well as the youngest and oldest ages obtained (Fig.

11b) from each sample indicate that the rocks were probably emplaced during multiple magmatic pulses. The youngest ages of c. 4 Ma are possibly magmatic, but could be affected by a hydrothermal or metamorphic overprint, related to contemporaneous S-type magmatism. The I-type rocks (Chappell & White, 1974, 2001; White & Chappell, 1983; Frost et al., 2001) typically have a high content of mafic minerals and few inherited zircon cores. Field observations show small shear zones and deformed mafic enclaves in some areas.

This magmatic episode is unlikely to be related to crustal thickening and anatectic melting of Australian-derived continental crust suggested for the CAK suite by Polvé et al. (1997) and Elburg et al. (2003), which would be expected to result in crustal-derived S-type granitoids. Instead, we suggest that this group of I-type CAK rocks was formed by partial melting of the lower crust with compositions similar to the rocks of the HK suite. One HK sample (SJH07) dated in this study may represent the products of partial melting of the lower crust, or a metasomatised lithospheric mantle as interpreted by Elburg et al. (2003). The sample has a crystallization age of c. 7 Ma which is similar to some I-type CAK rocks. One inherited age of c. 11 Ma was obtained which may be derived from the partially melted protolith. This age is within the age ranges reported for the HK suite by Priadi (1993), Priadi et al. (1994) and Polvé et al. (1997) at 13-10 Ma and by Elburg et al. (2003) at 14-5 Ma. Another zircon age of c. 14 Ma was obtained from an I-type granitoid (SRH42), which suggests that basic to intermediate rocks of the HK suite were partially re-melted to form the granitic I-type CAK rocks, assuming the Middle Miocene K-Ar ages for HK suite are correct.

The youngest magmatic activity identified in this study produced granitic intrusions, including dykes, with S-type affinities (Chappell & White, 1974, 2001; White & Chappell, 1983; Frost et al., 2001) in the southern Neck and to the east of the Palu-Koro Fault. CL images from all young zircons with rims show bright homogeneous rims, dark rims and rims with oscillatory zoning. Mid Pliocene weighted mean crystallization ages of 3.14 ± 0.18 Ma and 2.95 ± 0.07 Ma were calculated from SHRIMP analyses of zircon rims. Weighted mean ages calculated from S-type granitoids analyzed by LA-ICP-MS (Fig. 11a) are between 4 and 3 Ma. The oldest and youngest ages obtained from each sample (Fig. 11b) indicate several possible magmatic pulses from c. 5 Ma to 2.5 Ma. However, the youngest ages obtained could include those affected by a hydrothermal or

metamorphic overprint, which is indicated by coeval metamorphic ages obtained from zircon rims of gneisses (Gn46, Gn48, Gn50, SJH11_99).

Oscillatory zoned rims are typical of melt-derived zircon growth around xenocrysts and are interpreted as evidence for a Pliocene magmatic event at c. 4-3 Ma. These granitoids have inherited Cretaceous, Jurassic, Triassic and older zircon ages suggested to be reworked detrital grains in sediments that were the source rocks for the melts.

Identification of a very young phase of magmatism is important for the interpretation of cross-cutting relationships of dykes and metamorphic fabrics. Previous studies of the timing of ductile deformation in the Palu Metamorphic Complex suggested Late Cretaceous recrystallization in a subduction zone at the Sundaland margin (Parkinson et al., 1998) or an Eocene to Early Oligocene age (Watkinson, 2011). Abundant Triassic ages from oscillatory zoned zircons of gneisses in mid Central Sulawesi dated by this study suggest a granitoid protolith which was later metamorphosed to a gneiss. These granitoids must have intruded a basement, which suggests some Australian Paleozoic basement rocks could be present in Western Sulawesi. However, although there are some ultra-high pressure and high pressure rocks (de Roever, 1947, 1955) in Sulawesi that formed during collision in the Late Cretaceous or Early Miocene (Wakita et al., 1996; Parkinson et al., 1998; Kadarusman et al., 2001, 2002, 2005), the metamorphic rocks dated in this study are much younger than previously proposed.

CL images of zircons from the gneisses show patchy internal structures and convolute rims, which are indicative of medium- to high-grade metamorphic recrystallization (Corfu et al., 2003). The Th/U ratio is generally low for these zircons and, in combination with their internal structure, points to a metamorphic origin. Zircon rims have similar ages to the mid Pliocene melt rims in the granite dykes (Fig. 11a, b). The distribution of ages of zircon rims from the gneisses and the granitic bodies and coeval dykes is very similar and suggests crystallization of the granitoid intrusions during metamorphism. A metamorphic and magmatic connection is likely as the granitoid rocks intrude the strongly deformed metamorphic rocks. Macroscopically undeformed granitic dykes have ambiguous Th/U ratios, possibly influenced by Th-rich minerals, and show little deformation in thin sections, such as undulose quartz grains with subgrain formation and dynamic recrystallization with grain boundary migration.

Various factors, such as partitioning of Th and/or U into different minerals (e.g. Th in monazite) or enrichment of U in metamorphic fluids can influence the Th/U ratio (Ahrens, 1965; Ahrens et al., 1967; Rubatto et al., 1999).

Contemporaneous metamorphism and magmatism could be explained by contact metamorphism at the contact of plutons. However, these metamorphic rocks would be expected to be schists with a fine-grained contact metamorphic texture. The metamorphic ages reported in this study at c. 3.6 Ma were analyzed from gneisses of the PMC which are foliated and intensely folded. Some schists of the metapelite unit are biotite hornfelses with a contact metamorphic fabric. However, others show a later metamorphism resulting in a cleavage. Most of the schists from the PMC are as strongly deformed as the gneisses, and are cut by mylonitic shear zones in places, suggesting regional metamorphism after contact metamorphism.

Alternatively, a link between magmatism and metamorphism could be the result of crustal thickening following collision. However, the short time interval of the metamorphism and S-type magmatism conflict with a compressional setting in which radiogenic heating following crustal thickening would require a long time to produce high-grade metamorphic rocks, including migmatites, and magmatism. Instead, an extensional setting can explain both metamorphism of the mid to lower crustal rocks, as well as decompressional melting and ductile deformation along shear zones. Therefore, the co-occurrence of magmatism and metamorphism in the mid Pliocene is suggested to have occurred during an extensional phase. Extension initiated rapid uplift and exposure of strongly deformed lower crustal rocks in mylonitic shear zones. Subsequent decompression triggered the youngest phase of magmatism. Post-crystallisation deformation of some granites, including ~ N-S oriented boudinage of dykes and faulting, may be related to deformation associated with the NNW-trending active Palu-Koro Fault. Dating of metamorphic fabrics of the Palu Metamorphic Complex by Ar-Ar analysis of micas and amphiboles as well as low-temperature thermochronology on granitic rocks using Ar-Ar and (U-Th-Sm)-He techniques indicate contemporaneous deformation and rapid exhumation in the mid Pliocene (Hennig, 2014).

6. Conclusions

Gneisses and granitoid intrusions in western Sulawesi have zircons with abundant Mesozoic and Mesoproterozoic ages, some Paleozoic ages, and very rare Archean ages. The age populations differ significantly from those reported from East Java (Smyth et al., 2007, 2008). East Java zircons have a large proportion of Archean ages, and resemble zircon populations from Australia indicating an origin in the western part of the Australian margin of Gondwana. However, the western Sulawesi zircon ages, with dominant Mesoproterozoic and Triassic peaks, are similar to those reported from the Bird's Head (Gunawan et al., 2012; Gunawan, 2013). Therefore, before rifting, the NW Sulawesi terrane (NWS) is suggested to have been located in the inner part of the Banda Embayment south of the Bird's Head area (Fig. 13).

Some metapelites of the PMC contain Cretaceous zircons interpreted to have been derived from volcanogenic protoliths of Sundaland origin. Cretaceous zircon ages similar to those of the PMC were identified in the Pinoh Metamorphics and Schwaner intrusions in Borneo (Davies, 2013; Davies et al., 2014) and are likely to be the source of Cretaceous detrital zircons of NW Sulawesi.

Late Eocene to Early Oligocene detrital zircons are suggested to have been derived from magmatic rocks related to rifting of the Makassar Straits. The presence of Eocene zircons in some of the metamorphic rocks shows the metamorphism of these PMC metapelites is much younger than previously inferred, and they cannot be Mesozoic or older Australian-derived basement rocks.

During the Neogene there were several magmatic episodes. The HK suite is the oldest, based on K-Ar dating (Priadi et al., 1994; Polvé et al., 1997; Elburg et al., 2003) and had begun by c.14-13 Ma. One HK rock analyzed in this study has an age of 7 Ma and contains one inherited grain of c. 11 Ma. We suggest the HK suite was melted to form the I-type CAK rocks, based on an inherited zircon age of c. 14 Ma in an I-type CAK rock.

I-type and silica-rich I-type CAK magmatism took place between c. 8.5 and 4 Ma. Granites, granodiorites and diorites can be traced for c. 500 km along the west side of the northern Neck and southwards along the west side of the Palu-Koro Fault as far as Mamasa in southern West Sulawesi.

S-type magmatism started after I-type magmatism, and occurred between c. 5 and 2.5 Ma. Inherited ages, including a significant Mesozoic population and scattered Precambrian, Paleozoic and Paleogene ages, are similar to those from the gneisses, and suggest partial melting of the gneisses to form the S-type granitoids.

A metamorphic event in the Pliocene (c. 3.6 Ma) is recorded by dark or bright zircon rims of gneisses and some granites. This metamorphism was contemporaneous with S-type magmatism and is interpreted as due to extension.

Sulawesi has generally been interpreted as the product of convergence and collision in the Cretaceous and Cenozoic, resulting in magmatism and metamorphism. However, despite its situation in a young convergent setting, NW Sulawesi illustrates the importance of melting and metamorphism in an extensional setting during the early stages of mountain building.

Acknowledgements

This study was funded by the SE Asia Research Group at Royal Holloway which is supported by a consortium of oil companies. Fieldwork in Indonesia was assisted by Institut Teknologi Bandung (ITB) and the State Ministry of Research and Technology (RISTEK). We thank Theo van Leeuwen, Tim Breitfeld and Lloyd White for helpful discussions, Martin Rittner (UCL/Birkbeck College) for help and support at the LA-ICP-MS facility, Matthew Thirlwall and Christina Manning for assistance with geochemical analyses, and Bin Fu (PRISE, ANU, Australia) for cathodoluminescence imaging. Special thanks to Afif Saputra (INPEX) for great assistance during fieldwork. Mike Cottam and Eldert Advokaat are gratefully acknowledged for obtaining additional samples. The manuscript benefited greatly from comments by Tony Barber and an anonymous reviewer.

References

Ahlburg, J., 1913. Versuch einer geologischen Darstellung der Insel Celebes. Neue Folge Band 12, 172 pp.

Ahrens, L. H., 1965. Some observations on the uranium and thorium distributions in accessory zircon from granitic rocks. Geochimica et Cosmochimica Acta 29, 711-716.

Ahrens, L. H., Cherry, R. D., Erlank, A. J., 1967. Observations on the Th-U relationship in zircons from granite rocks and from kimberlites. Geochimica et Cosmochimica Acta 31, 2379-2387.

Andersen, T., 2002. Correction of common lead in U–Pb analyses that do not report ^{204}Pb. Chemical Geology 192, 59–79.

Apandi, T., 1977. Geological map of the Kotamobagu Quadrangle, North Sulawesi - 1: 250 000. Geological Survey of Indonesia, Directorate of Mineral Resources, Geological Research and Development Centre, Bandung, Indonesia.

Black, L. P., Kamo, S. L., Allen, C. M., Davis, D. W., Aleinikoff, J. N., Valley, J. W., Mundil, R., Campbell, I. H., Korsch, R. J., Williams, I. S., Foudoulis, C., 2004. Improved $^{206}Pb/^{238}U$ microprobe geochronology by the monitoring of a trace-element-related matrix effect; SHRIMP, ID-TIMS, ELA-ICP-MS and oxygen isotope documentation for a series of zircon standards. Chemical Geology 205, 115–140.

Brouwer, H. A., 1934. Geologische onderzoekingen op het eiland Celebes. Verhandelingen Koninklijk Nederlands Geologisch en Mijnbouwkundig Genootschap, Geologische Serie V, 10, 39-218.

Calvert, S. J., Hall, R., 2007. Cenozoic evolution of the Lariang and Karama regions, North Makassar Basin, western Sulawesi, Indonesia. Petroleum Geoscience 13, 4, 353-368.

Chappell, B. W., White, A. J. R., 1974. Two contrasting granite types. Pacific Geology 8, 173-174.

Chappell, B. W., White, A. J. R., 2001. Two contrasting granite types: 25 years later. Australian Journal of Earth Sciences 48, 489-499.

Corfu, F., Hanchar, J. M., Hoskin, P. W. O., Kinny, P. D., 2003. Atlas of zircon textures. Reviews in Mineralogy and Geochemistry, 53, 1, 469–500.

Cox, K. G., Bell, J. D., Pankhurst, R. J., 1979. The Interpretation of Igneous Rocks. George Allen & Unwin, London, 450 pp.

Davies, L., 2013. SW Borneo Basement: Age, origin and character of igneous and metamorphic rocks from the Schwaner Mountains. Ph.D. thesis, Royal Holloway University of London, 391 pp.

Davies, L., Hall, R., Armstrong, R., 2014. Cretaceous crust in SW Borneo: petrographical, geochemical and geochronological constraints from the Schwaner Mountains. Proceedings Indonesian Petroleum Association, 38th Annual Convention and Exhibition, IPA14-G-025.

de la Roche, H., Leterrier, J., Grandclaude, P., Marchal, M., 1980. A classification of volcanic and plutonic rocks using R1R2-diagram and major-element analyses –Its relationships with current nomenclature: Chemical Geology 29, 183-210.

de Roever, W. P., 1947. Igneous and metamorphic rocks in eastern central Celebes. In: Brouwer, H. A. (Ed.), Geological Exploration of the Island of Celebes. Amsterdam, North Holland Publishing Co., 65-173.

de Roever, W. P., 1955. Genesis of jadeite by low-temperature metamorphism. American Journal of Science 253, 283-298.

Egeler, C. G., 1947. Contribution to the petrology of the metamorphic rocks of western Celebes. Geological Expedition to the Island of Celebes, University of Amsterdam, 185-346.

Elburg, M., Foden, J., 1999. Sources for magmatism in Central Sulawesi: Geochemical and Sr-Nd-Pb constraints. Chemical Geology 156, 67–93.

Elburg, M., van Leeuwen, T., Foden, J., Muhardjo, 2003. Spatial and temporal isotopic domains of contrasting igneous suites in Western and Northern Sulawesi, Indonesia. Chemical Geology 199, 3-4, 243-276.

Frost, B. R., Barnes, C. G., Collins, W. J., Arculus, R. J., Ellis, D. J., Frost, C. D., 2001. A geochemical classification for granitic rocks. Journal of Petrology 42, 2033-2048.

Gunawan, I., 2013. Mesozoic and Cenozoic siliciclastic sedimentary rocks of the Bird's Head of New Guinea, Indonesia. Ph.D. Thesis, Royal Holloway University of London, 472 pp.

Gunawan, I., Hall, R., Sevastjanova, I., 2012. Age, character and provenance of the Tipuma Formation, West Papua: New Insights from detrital zircon dating. Proceedings Indonesian Petroleum Association, 36th Annual Convention. IPA12-G-027, 1-14.

Haile, N. S., McElhinny, M. W., McDougall, I., 1977. Palaeomagnetic data and radiometric ages from the Cretaceous of West Kalimantan (Borneo), and their significance in interpreting regional structure. Journal of the Geological Society of London 133, 133-144.

Hall, R., 1996. Reconstructing Cenozoic SE Asia. In: Hall, R., Blundell, D. J. (Eds.), Tectonic Evolution of SE Asia. Geological Survey of London Special Publication 106, 153-184.

Hall, R., 2002. Cenozoic geological and plate tectonic evolution of SE Asia and the SW Pacific: computer-based reconstructions, model and animations. Journal of Asian Earth Sciences 20, 4, 353-434.

Hall, R., 2011. Australia-SE Asia collision: plate tectonics and crustal flow. In: Hall, R., Cottam, M. A., Wilson, M. E. J. (Eds.), The SE Asian Gateway: History and Tectonics of the Australia-Asia collision. Geological Society of London Special Publication 355, 75-109.

Hall, R., 2012. Late Jurassic-Cenozoic reconstructions of the Indonesian region and the Indian Ocean. Tectonophysics 570-571, 1-41.

Hall, R., Morley, C. K., 2004. Sundaland Basins. In: Clift, P., Wang, P., Kuhnt, W., Hayes, D. E. (Eds.), Continent-Ocean Interactions within the East Asian Marginal Seas. AGU Geophysical Monograph 149, 55-85.

Hall, R., Clements, B., Smyth, H. R., 2009. Sundaland: basement character, structure and plate tectonic development. Proceedings Indonesian Petroleum Association, 33rd Annual Convention. IPA09-G-134, 1-27.

Hall, R., Sevastjanova, I., 2012. Australian crust in Indonesia. Australian Journal of Earth Sciences 59, 6, 827-844.

Hamilton, W., 1979. Tectonics of the Indonesian region. U. S. Geological Survey Professional Paper 1078, 345 pp.

Hennig, 2014. Age, origin and exhumation history of magmatic and metamorphic rocks of NW Sulawesi, Indonesia. Ph.D. thesis, Royal Holloway University of London, 584 pp.

Hutchison, C. S., 1973. Tectonic evolution of Sundaland: a Phanerozoic synthesis. Bulletin of the Geological Society of Malaysia 6, 61-86.

Hutchison, C. S., 1989. Geological evolution of South-East Asia. Oxford Monographs on Geology and Geophysics, 13, Clarendon Press, 376 pp.

Kadarusman, A., Brueckner, H., Yurimoto, H., Parkinson, C. D., Maruyama, S., 2001. Geochemistry and Sm-Nd age dating of garnet peridotites from central Sulawesi and their implication to the Neogene Collision in Eastern Indonesia [abs.]. EOS (Transactions, American Geophysical Union) 82, 48, p. F1641.

Kadarusman, A., Sopaheluwakan, J., van Leeuwen, T. M., 2002. Eclogite, garnet peridotite, granulite and associated high-grade rocks from the Palu-Koro region, Central Sulawesi, Indonesia: An example of mantle and crust interactions in young orogenic belt [abs.].EOS (Transactions, American Geophysical Union) 83, 48, F1182.

Kadarusman, A., van Leeuwen, T., Soeria-Atmadja, R., 2005. Discovery of eclogite in the Palu region, Central Sulawesi, and its implication for the tectonic evolution of Sulawesi. Majalah Geologi Indonesia 20, 80-89.

Kavalieris, I., van Leeuwen, T. M., Wilson, M., 1992. Geological setting and styles of mineralization, north arm of Sulawesi, Indonesia. Journal of Southeast Asian Earth Sciences 7, 113-130.

Ludwig, K. R., 2003. User's Manual for Isoplot 3.00. Berkeley Geochronology Center: Berkeley, CA, 70 pp.

Metcalfe, I., 1988. Origin and assembly of Southeast Asian continental terranes. In: Audley-Charles, M. G., Hallam, A. (Eds.), Gondwana and Tethys 37, 101-118.

Metcalfe, I., 1990. Allochthonous terrane processes in Southeast Asia. Philosophical Transactions Royal Society of London A331, 625-640.

Metcalfe, I., 1996. Pre-Cretaceous Evolution of SE Asian Terranes. In: Hall, R., Blundell, D. J. (Eds.), Tectonic Evolution of SE Asia. Geological Survey of London Special Publication 106, 97-122.

Metcalfe, I., 2009. Late Palaeozoic and Mesozoic tectonic and palaeogeographical evolution of SE Asia. In: Buffetaut, G., Cuny, Le Loeuff, J., Suteethorn, V. (Eds.), Late Palaeozoic and Mesozoic Ecosystems in SE Asia. Geological Society of London Special Publication 315, 7-23.

Metcalfe, I., 2011. Palaeozoic-Mesozoic History of SE Asia. In: Hall, R., Cottam, M. A., Wilson, M. E. J. (Eds.), The SE Asian Gateway: History and Tectonics of the Australia-Asia collision. Geological Society of London Special Publication 355, 7-35.

Muir, R. J., Ireland, T. R., Weaver, S. D., Bradshaw, J. D., 1996. Ion microprobe dating of Paleozoic granitoids: Devonian magmatism in New Zealand and correlations with Australia and Antarctica. Chemical Geology (Isotope Geoscience Section) 127, 191–210.

Neumann, N. L., Fraser, G. F. (Eds.), 2007.Geochronological synthesis and time-space plots for Proterozoic Australia. Geoscience Australia Record 2007/06, Geoscience Australia, Canberra, ACT, 216 pp.

Parkinson, C., 1998a. Emplacement of the East Sulawesi Ophiolite: evidence from subophiolite metamorphic rocks. Journal of Asian Earth Sciences 16, 13-28.

Parkinson, C., 1998b. An outline of the petrology, structure and age of the Pompangeo Schist Complex of central Sulawesi, Indonesia. Island Arc 7, 231-245.

Parkinson, C. D., Miyazaki, K., Wakita, K., Barber, A. J., Carswell, D. A., 1998. An overview and tectonic synthesis of the pre-Tertiary very-high-pressure metamorphic and associated rocks of Java, Sulawesi and Kalimantan, Indonesia. The Island Arc 7, 184-200.

Passchier, C. W., Trouw, R. A. J., 1996. Microtectonics. Springer Verlag, Berlin, 289 pp.

Pearce, N. J. G., Perkins, W. T., Westgate, J. A., Gorton, M. P., Jackson, S. E., Neal, C. R., Cenery, S. P., 1997. A compilation of new and published major and trace element data for NIST SRM 610 and NIST SRM 612 glass reference materials. Geostandards Newsletter 21, 115–144.

Peccerillo, R., Taylor, S. R., 1976. Geochemistry of Eocene calc-alkaline volcanic rocks from the Kastamonu area, northern Turkey. Contributions to Mineralogy and Petrology 58, 63-81.

Polvé, M., Maury, R. C., Bellon, H., Rangin, C., Priadi, B., Yuwono, S., Joron, J. L., Atmadja, R. S., 1997. Magmatic evolution of Sulawesi (Indonesia): Constraints on the Cenozoic geodynamic history of the Sundaland active margin. Tectonophysics 272, 1, 69-92.

Pownall, J. M., Hall, R., Watkinson, I. M., 2013. Extreme extension across Seram and Ambon, eastern Indonesia: evidence for Banda slab rollback. Solid Earth 4, 277–314.

Pownall, J. M., Hall, R., Armstrong, R. A., Forster, M. A., 2014. Earth's youngest known ultrahigh-temperature granulites discovered on Seram, eastern Indonesia. Geology 42, 279-282.

Priadi, B., 1993. Geochemie du magmatism de l'ouest et du nord de Sulawesi, Indonesie. Ph.D. Thesis, L'Université Paul Sabatier de Toulouse, 293 pp.

Priadi, B., Polvé, M., Maury, R. C., Bellon, H., Soeria-Atmadia, R., Joron, J. L., Cotten, J., 1994. Tertiary and Quaternary magmatism in Central Sulawesi: chronological and petrological constraints. Journal of Southeast Asian Earth Sciences 9, 81-93.

Ratman, N., 1976. Geological map of the Tolitoli Quadrangle, North Sulawesi - 1:250,000, Geological Research and Development Centre, Bandung, Indonesia.

Ratman, N., Atmawinata, S., 1993. Geology of the Mamuju Quadrangle Sulawesi – 1:250,000, Geological Research and Development Centre, Bandung, Indonesia.

Rubatto, D., Gebauer, D., Compagnoni, R., 1999. Dating of eclogites-facies zircons: the age of Alpine metamorphism in the Sesia-Lanzo Zone (Western Alps). Earth and Planetary Science Letters 167, 141-158.

Rubatto, D., 2002. Zircon trace element geochemistry: distribution coefficients and the link between U-Pb ages and metamorphism. Chemical Geology 184, 123-138.

Sambridge, M. S., Compston, W., 1994. Mixture modeling of multi-component data sets with application to ion-probe zircon ages. Earth and Planetary Science Letters 128, 373-390.

Sarasin, P., Sarasin, F., 1901. Material zur Naturgeschichte der Insel Celebes: Bd. Entwurf einer geografisch- geologischen Beschreibung der Insel Celebes. Anhang: Untersuchung einiger Gesteinssuiten, gesammelt in Celebes von P. und F. Sarasin, von Schmidt. Vol. 4. CW Kreidel's Verlag, Wiesbaden, Deutschland.

Sevastjanova, I., Clements, B., Hall, R., Belousova, E. A., Griffin, W. L., Pearson, N., 2011. Granitic magmatism, basement ages, and provenance indicators in the Malay Peninsula: Insights from detrital zircon U-Pb and Hf-isotope data. Gondwana Research 19, 1024-1039.

Simandjuntak, T. O., Rusmana, E., Surono, Supandjono, J. B., 1991. Geological map of the Malili Quadrangle, Sulawesi –1:250,000. Geological Research and Development Centre, Bandung, Indonesia.

Simandjuntak, T. O., Surono, Supandjono, J. B., 1997. Geological map of the Poso Quadrangle, Sulawesi –1:250,000. Geological Research and Development Centre, Bandung, Indonesia.

Sircombe, K. N., Freeman, M. J., 1999. Provenance of detrital zircons on the Western Australia coastline – Implications for the geologic history of the Perth basin and denudation of the Yilgarn craton. Geology 27, 10, 879-882.

Sláma, J., Kosler, J., Condon, D. J., 2008. Plešovice zircon–A new natural reference material for U-Pb and Hf isotopic microanalysis. Chemical Geology 249, 1-35.

Smyth, H. R., Hamilton, P. J., Hall, R., Kinny, P. D., 2007. The deep crust beneath island arcs: inherited zircons reveal a Gondwana continental fragment beneath East Java, Indonesia. Earth and Planetary Science Letters 258, 269-282.

Smyth, H. R., Hall, R., Nichols, G. J., 2008. Cenozoic volcanic arc history of East Java, Indonesia: the stratigraphic record of eruptions on an active continental margin. Geological Society of America Special Papers 436, 199-222.

Sopaheluwakan, J., Kadarusman, A., Priadi, B., Utoyo, H., 1995. The nature of the basement rocks in the Palu region, Central Sulawesi: The newly found eclogite and its regional implication. Proceedings of the Sixth International Congress on Pacific Neogene Biostratigraphy and IGCP –355, Neogene Evolution of Pacific: Biotic, Oceanographic and Tectonic Development, Kyoto Institute of Natural History, Kyoto, Japan, 73–79.

Spakman, W., Hall, R., 2010. Surface deformation and slab-mantle interaction during Banda arc subduction rollback. Nature Geoscience 3, 562–566.

Streckeisen, A., 1974. Classification and nomenclature of plutonic rocks. Geologische Rundschau 63, 773-786.

Sukamto, R., 1973. Reconnaissance geologic map of Palu Area, Sulawesi – 1:250,000. Geological Research and Development Centre, Bandung, Indonesia.

Sukido, D., Sukarna, Sutisna, K., 1993. Geological Map of the Pasangkayu Quadrangle, Sulawesi –1:250,000. Geological Research and Development Centre, Bandung, Indonesia.

Tera, F., Wasserburg, G. J., 1972. U-Th-Pb systematics in three Apollo 14 basalts and the problem of initial Pb in lunar rocks. Earth and Planetary Science Letters 14, 281-304.

van Hattum, M. W. A., Hall, R., Pickard, A. L., Nichols, G. J., 2013. Provenance and geochronology of Cenozoic sandstones of northern Borneo. Journal of Asian Earth Sciences 76, 266-282.

van Leeuwen, T. M., Taylor, R., Coote, A., Longstaffe, F. J., 1994. Porphyry molybdenum mineralization in a continental collision setting at Malala, northwest Sulawesi, Indonesia. Journal of Geochemical Exploration 50, 279-315.

van Leeuwen, T. M., Muhardjo, 2005. Stratigraphy and tectonic setting of the Cretaceous and Paleogene volcanic-sedimentary successions in northwest Sulawesi, Indonesia: implications for the Cenozoic evolution of Western and Northern Sulawesi. Journal of Asian Earth Sciences 25, 481-511.

van Leeuwen, T. M., Allen, C. M., Kadarusman, A., Elburg, M., Palin, J. M., Muhardjo, Suwijanto, 2007. Petrologic, isotopic, and radiometric age constraints on the origin and tectonic history of the Malino Metamorphic Complex, NW Sulawesi, Indonesia. Journal of Asian Earth Sciences 29, 751-777.

Wakita, K., Sopaheluwakan, J., Miyazaki, K., Zulkarnain, I., Munasri, 1996.Tectonic Evolution of the Bantimala Complex, South Sulawesi, Indonesia. In: Hall, R., Blundell, D. J. (Eds.), Tectonic Evolution of SE Asia. Geological Society of London Special Publication 106, 353-364.

Watkinson, I. M., 2011. Ductile flow in the metamorphic rocks of central Sulawesi. In: Hall, R., Cottam, M. A., Wilson, M. E. J. (Eds.), The SE Asian Gateway: History and Tectonics of the Australia-Asia collision. Geological Society of London Special Publication 355, 157-176.

Weissel, J. K., 1980. Evidence for Eocene oceanic crust in the Celebes Basin. In: Hayes, D. E., (Ed.), The Tectonic and Geologic Evolution of Southeast Asian Seas and Islands. American Geophysical Union, Geophysical Monograph Series 23, 37-47.

Wetherill, G. W., 1956. Discordant uranium-lead ages. Transactions of the American Geophysical Union, 37, 320-326.

White, A. J. R., Chappell, B. W., 1983. Granitoid rocks and their distribution in the Lachlan fold belt, southeastern Australia. Geological Society of America Memoir 159, 21-34.

White, L. T., Ireland, T. R., 2012. High-uranium matrix effect in zircon and its implications for SHRIMP U-Pb age determinations. Chemical Geology 306, 78-91.

Williams, I. S., 1998. U–Th–Pb geochronology by ion microprobe. In: McKibben, M. A., Shanks III, W. C., Ridley, W. I. (Eds.), Applications of Microanalytical Techniques to Understanding Mineralizing Processes: Reviews in Economic Geology 7, 1–35.

Figure captions:

Fig. 1: Geological map of west Central Sulawesi modified from previous studies (Sukamto, 1973; Ratman, 1976; Sukido et al., 1993; Ratman & Atmawinata, 1993; Simandjuntak et al., 1991, 1997; van Leeuwen & Muhardjo, 2005 and Calvert & Hall, 2007). The map includes our own field observations. Inset map shows the five main lithotectonic provinces of Sulawesi. Abbreviations: PMC - Palu Metamorphic Complex; MMC - Malino Metamorphic Complex; PSC - Pompangeo Schist Complex; G – Gumbasa Metamorphic Complex; W - Wana Metamorphic Complex; K - Karossa Metamorphic Complex; T – Tinombo Formation; L – Latimojong Formation; P – Papayato Volcanics.

Fig. 2: Geochemical classification of granitoid rocks from west Central Sulawesi. a) SiO_2 vs. K_2O diagram after Peccerillo & Taylor (1976). Previous analyses are shown with grey symbols (Priadi, 1993; Priadi et al., 1994; Elburg & Foden, 1999; Elburg et al., 2003) and were used to define three subgroups: a High Potassium (HK) Suite, a High Potassium Calc-alkaline (CAK) Suite, and a Low Potassium Calc-alkaline (CA) suite. Samples analyzed in this study are shown in color and are subdivided into I-type and silica-rich I-type (blue) and S-type (red) rocks. b) Total alkali vs. silica (TAS) diagram (Cox et al., 1979) showing the distinction between the CAK and HK suites. Almost all the samples of this study fall in the Granodiorite and Granite fields and have a CAK character.

Fig. 3: Sample location map. Colored symbols show I- and S-type granitoids and diorites. All S-type rocks are found east of the Palu-Koro Fault. Samples shown in brackets and in italics are undated; all other samples were dated by U-Pb zircon analyses.

Fig. 4: Outcrop, hand specimen and thin section images for Neogene S-type (a-d) and I-type (e-h) granitoids. a) Granite dyke (SJH01) intruding schists of the Palu Metamorphic Complex between Tawaeli and Toboli. The contact is irregular and faulted, and the dyke is cut by subvertical and subhorizontal fractures. b) Hand specimen of a biotite granite from the north part of the Bada Basin with biotite restites (SJH11_121). c) and d) Thin section photographs (SJH11_122) under plane and crossed polarized light showing quartz, plagioclase, turbid K-feldspar and biotite with chlorite alteration. e) Granitoid

intrusions of the 'Dondo Suite' form high mountains in the northern Neck. f) Granodiorite with pink K-feldspar and abundant green amphibole needles (SJH11_45). g) Thin section photograph of a granodiorite (SJH03) with hyp- to idiomorphic amphibole and biotite (crossed polarized light). h) Thin section photograph of a large K-feldspar phenocryst in a granite from the Neck (SJH05).

Fig. 5: Zircon ages from schists of the PMC. a) Age histogram with probability density plot and Concordia diagram showing a Cretaceous population that ranges from c. 67 to 120 Ma (SJH11_1214). b) Histogram with probability density plot and Tera-Wasserburg Concordia diagram showing a narrow peak of Late Eocene to Early Oligocene ages (SJH11_05).

Fig. 6: Zircon ages from gneisses of the PMC. a) Concordia diagram showing a significant Triassic population (Gn49). b) Combined histogram with probability density plot of all gneiss samples from the PMC (Gn46, Gn48, Gn49, Gn50). The Pliocene peak was obtained from zircon rims. c) Tera-Wasserburg Concordia diagram of metamorphic rim analyses (Gn46). d) CL image of zircons from sample Gn46. The yellow circles (c. 20 μm) mark the SHRIMP analytical sites. Spot numbers are listed in Supplementary Data File 4.

Fig. 7: Age histogram with probability density plot and Concordia diagram of zircon ages from a mid Central Sulawesi gneiss (SJH11_113) showing several age populations in the Mesoproterozoic, Paleozoic and Mesozoic which indicate reworking of different magmatic rocks into a detrital sediment that was the protolith of the gneiss.

Fig. 8: Age histogram with probability density plot, Tera-Wasserburg Concordia diagram and CL image showing zircon U-Pb ages from a mid Central Sulawesi gneiss (SJH11_99). The zircons show convolute disturbed cores, and metamorphic zircon rims at c. 3 Ma. The yellow circles (c. 10 μm) indicate the SHRIMP analyses with spot numbers listed in Supplementary Data File 4.

Fig. 9: Age histogram with probability density plot, Tera-Wasserburg Concordia diagram and CL images showing zircon U-Pb ages from a granite dyke from the Neck (SJH01). The zircons record dark and bright zircon rim growth at c. 3 Ma. The yellow

circles (c. 10 μm) indicate the SHRIMP analyses with spot numbers listed in Supplementary Data File 4.

Fig. 10: Age histogram with probability density plot, Tera-Wasserburg Concordia diagram and CL image showing zircon U-Pb ages from a granite dyke from mid Central Sulawesi (SJH11_103). Zircon cores are mantled by euhedral oscillatory zoned rims with ages of c. 3 Ma. The yellow circles (c. 10 μm) indicate the SHRIMP analyses with spot numbers listed in Supplementary Data File 4.

Fig. 11: Summary of all Neogene zircon U-Pb ages obtained from I-type, silica-rich I-type rocks and S-type rocks analyzed by SHRIMP or LA-ICP-MS. a) Diagram showing all weighted mean ages calculated from the youngest significant peak of each sample (Table 1). The magmatic samples were analyzed by LA-ICP-MS, except for sample SJH01 and SJH11_103, and metamorphic rim ages (SJH11_99, Gn46, Gn48, Gn50), which were analyzed by SHRIMP (2σ errors are displayed). b) Diagram showing weighted mean ages calculated from the youngest significant peak, and the range of ages obtained from each sample. The oldest and youngest ages were obtained by LA-ICP-MS (1σ errors are displayed) except for sample SJH01. For this sample the SHRIMP ages are plotted.

Fig. 12: Histogram and probability density plot showing all inherited zircon ages from metamorphic and S-type granitoid rocks. There are significant age populations (highlighted) in the Mesoproterozoic, Mesozoic, and Paleogene. A large number of Precambrian ages were obtained (n = 87) but only one Archean age. The Precambrian ages are very different from those obtained from East Java but resemble those from the Bird's Head, as discussed in the text.

Fig. 13: Reconstruction at 150 Ma, modified from Hall (2012), showing position of the Inner Banda (= NW Sulawesi) block shortly after Late Jurassic rifting from the Australian margin and at 90 Ma, at about the time of collision of the East Java-West Sulawesi (EJWS) and NW Sulawesi (NWS) blocks with the Sunda margin. Abbreviations: ExP – Exmouth Plateau, ScP – Scott Plateau, SWB – SW Borneo, EJWS – East Java-West Sulawesi, NWS – NW Sulawesi.

Fig. 14: Summary maps showing sources interpreted for NW Sulawesi detrital zircons on tectonic reconstructions by Hall (2012). a) Before rifting, NW Sulawesi was situated in the Inner Banda Embayment close to the Bird's Head, from which abundant Mesoproterozoic and (Permo-) Triassic zircons were derived. Mesoproterozoic and rare Archean zircons were derived from the Australian continent. b) NW Sulawesi was accreted to the Sundaland margin in the Late Cretaceous and was close to the SW Borneo block until the Early Eocene. Cretaceous zircons in NW Sulawesi were derived from volcanogenic and magmatic rocks in the Schwaner Mountains of Borneo. c) Magmatism and metamorphism associated with rifting of the Makassar Straits provided zircons that were eroded and deposited in NW Sulawesi during or after the Eocene.

Table captions:

Table 1: Sample locations and U-Pb zircon ages from LA-ICP-MS and SHRIMP analyses.

Table 2: XRF whole-rock analyses of the Neogene granitoids and diorites.

Supplementary Data Files:

Supplementary Data File 1: Concordia diagrams, Tera-Wasserburg Concordia diagrams and weighted mean age diagrams with probability density plots for all samples analyzed.

Supplementary Data File 2: ASI (alumina saturation index) diagram of Frost et al. (2001) showing the classification of Neogene magmatic rocks analyzed in this study into I-type, silica-rich I-type and S-type granitoids and diorites.

Supplementary Data File 3: Data tables of LA-ICP-MS analyses.

Supplementary Data File 4: Data tables of SHRIMP analyses.

Supplementary Data File 5: Histograms and probability density plots for all samples analyzed.

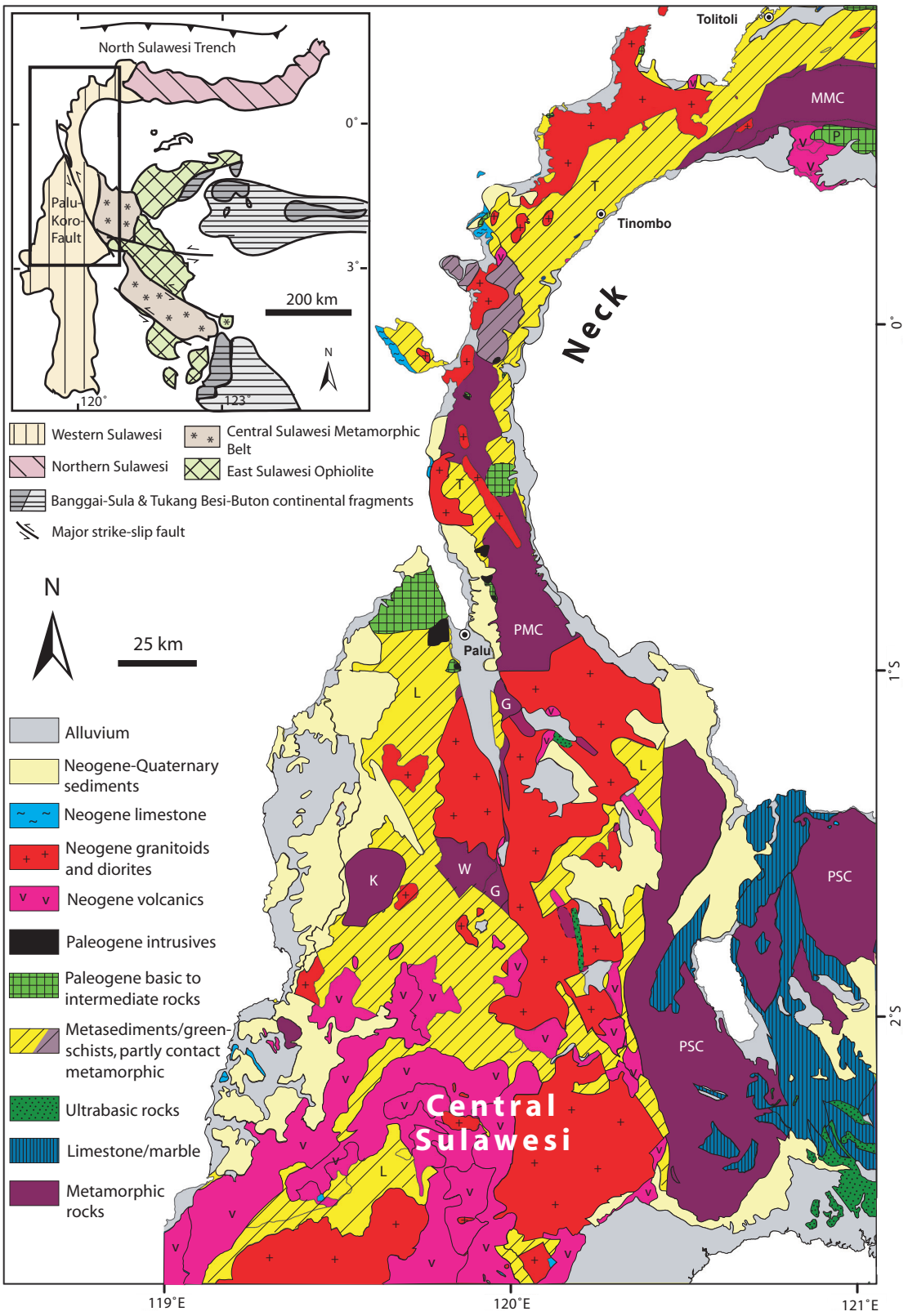
North Sulawesi Trench
Palu-Koro-Fault
0°
3°
200 km
N
120°
123°
Western Sulawesi
Northern Sulawesi
Banggai-Sula & Tukang Besi-Buton continental fragments
Major strike-slip fault
Central Sulawesi Metamorphic Belt
East Sulawesi Ophiolite
N
25 km
Alluvium
Neogene-Quaternary sediments
Neogene limestone
Neogene granitoids and diorites
Neogene volcanics
Paleogene intrusives
Paleogene basic to intermediate rocks
Metasediments/green-schists, partly contact metamorphic
Ultrabasic rocks
Limestone/marble
Metamorphic rocks
Tolitoli
MMC
Tinombo
Neck
PMC
Palu
PSC
PSC
Central Sulawesi
0°
1°S
2°S
119°E
120°E
121°E

Fig. 1

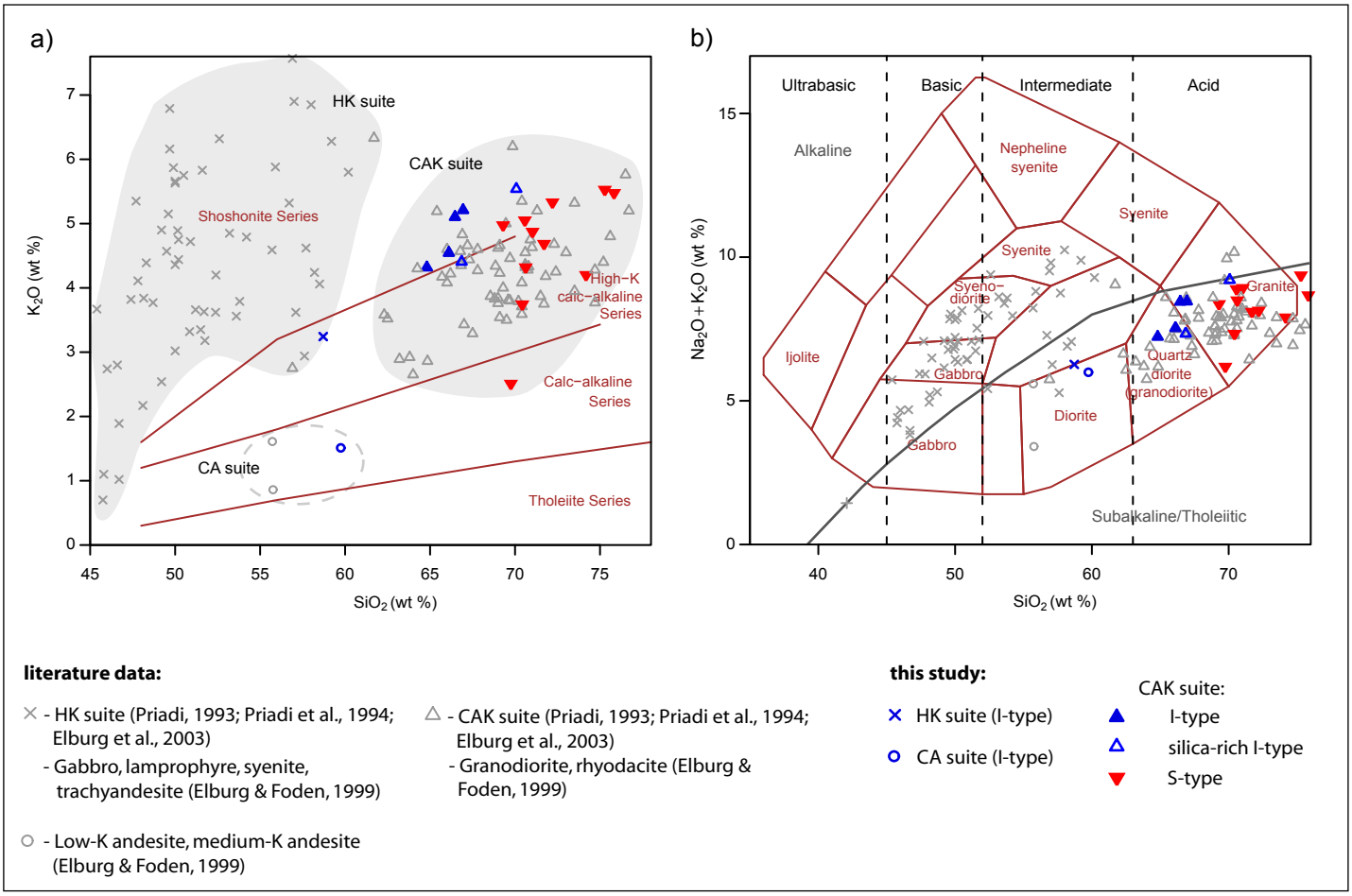

literature data:

× - HK suite (Priadi, 1993; Priadi et al., 1994; Elburg et al., 2003)
- Gabbro, lamprophyre, syenite, trachyandesite (Elburg & Foden, 1999)

△ - CAK suite (Priadi, 1993; Priadi et al., 1994; Elburg et al., 2003)
- Granodiorite, rhyodacite (Elburg & Foden, 1999)

○ - Low-K andesite, medium-K andesite (Elburg & Foden, 1999)

this study:

× HK suite (I-type)

○ CA suite (I-type)

CAK suite:
▲ I-type
△ silica-rich I-type
▼ S-type

Fig. 2

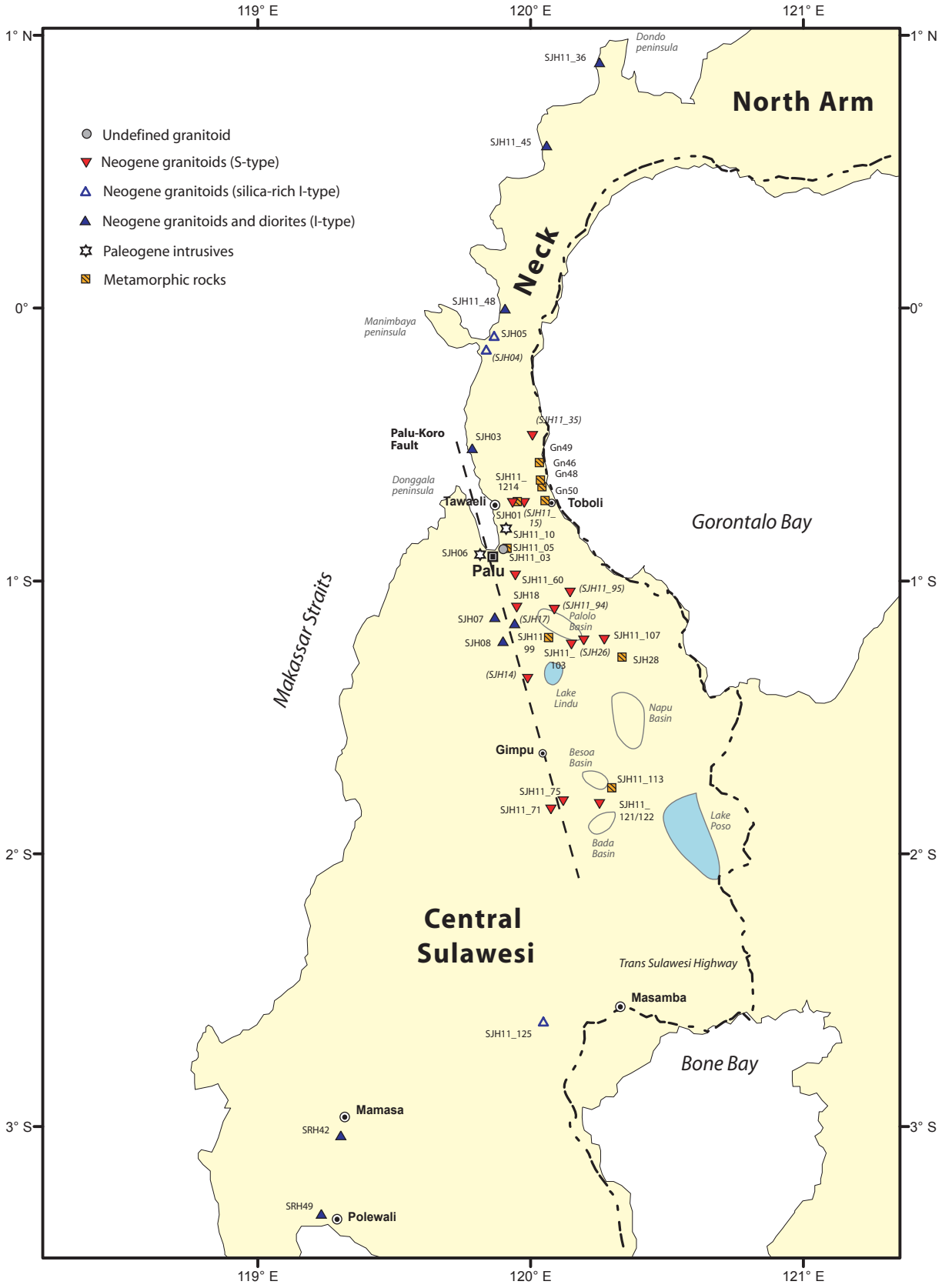
119° E
120° E
121° E
1° N
0°
1° S
2° S
3° S
Undefined granitoid
Neogene granitoids (S-type)
Neogene granitoids (silica-rich I-type)
Neogene granitoids and diorites (I-type)
Paleogene intrusives
Metamorphic rocks
North Arm
Neck
Dondo peninsula
SJH11_36
SJH11_45
SJH11_48
Manimbaya peninsula
SJH05
(SJH04)
Palu-Koro Fault
SJH03
(SJH11_35)
Gn49
Gn46
Gn48
Gn50
SJH11_ 1214
Donggala peninsula
Tawaeli
Toboli
SJH01
(SJH11_ 15)
SJH11_10
SJH11_05
SJH11_03
SJH06
Palu
Gorontalo Bay
Makassar Straits
SJH11_60
(SJH11_95)
SJH18
(SJH11_94)
Palolo Basin
SJH07
(SJH17)
SJH08
SJH11_ 99
SJH11_ 103
(SJH26)
SJH11_107
SJH28
(SJH14)
Lake Lindu
Napu Basin
Gimpu
Besoa Basin
SJH11_113
SJH11_75
SJH11_71
SJH11_ 121/122
Lake Poso
Bada Basin
Central Sulawesi
Trans Sulawesi Highway
Masamba
SJH11_125
Bone Bay
Mamasa
SRH42
SRH49
Polewali

Fig. 3

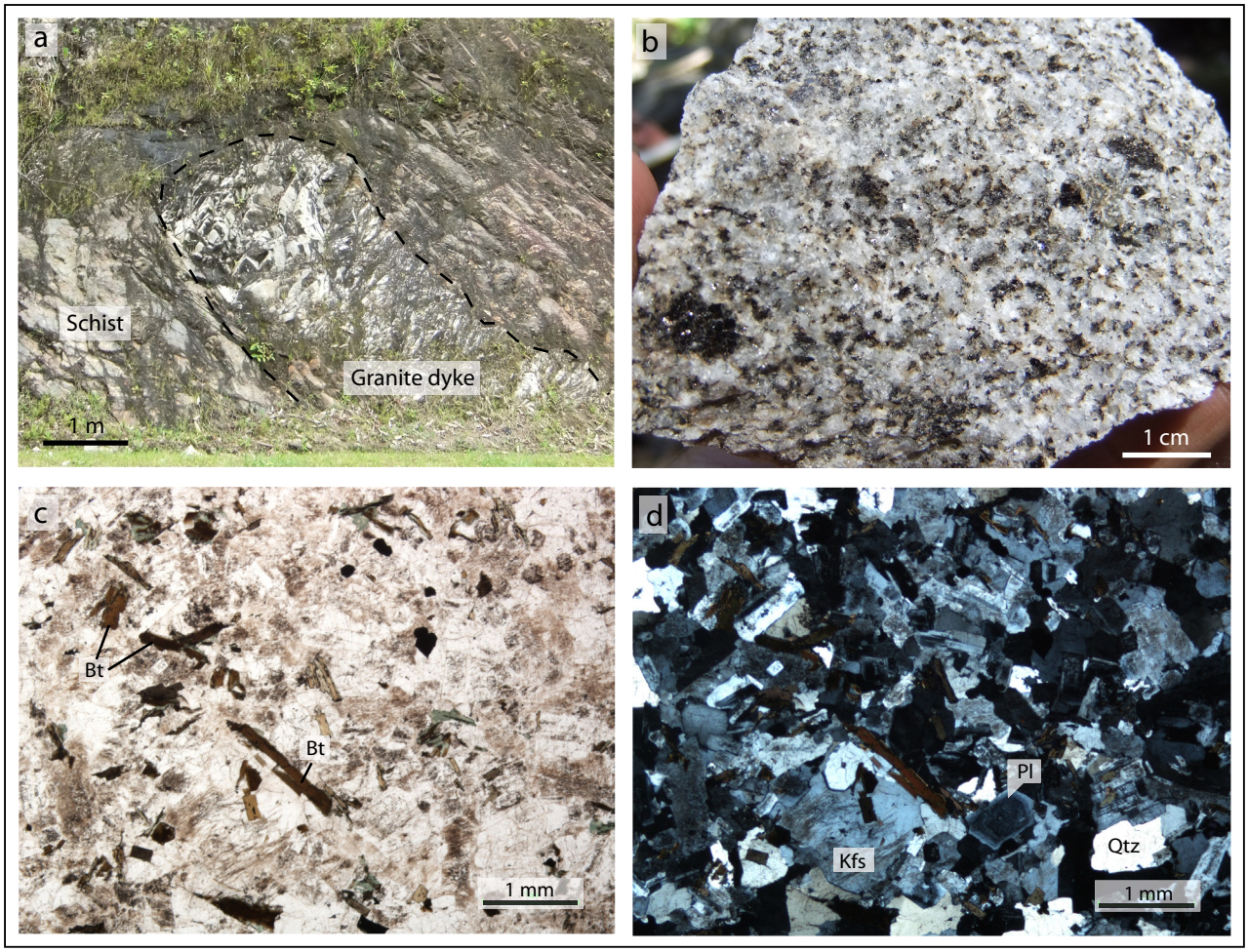
a
Schist
Granite dyke
1 m
b
1 cm
c
Bt
Bt
1 mm
d
Pl
Kfs
Qtz
1 mm

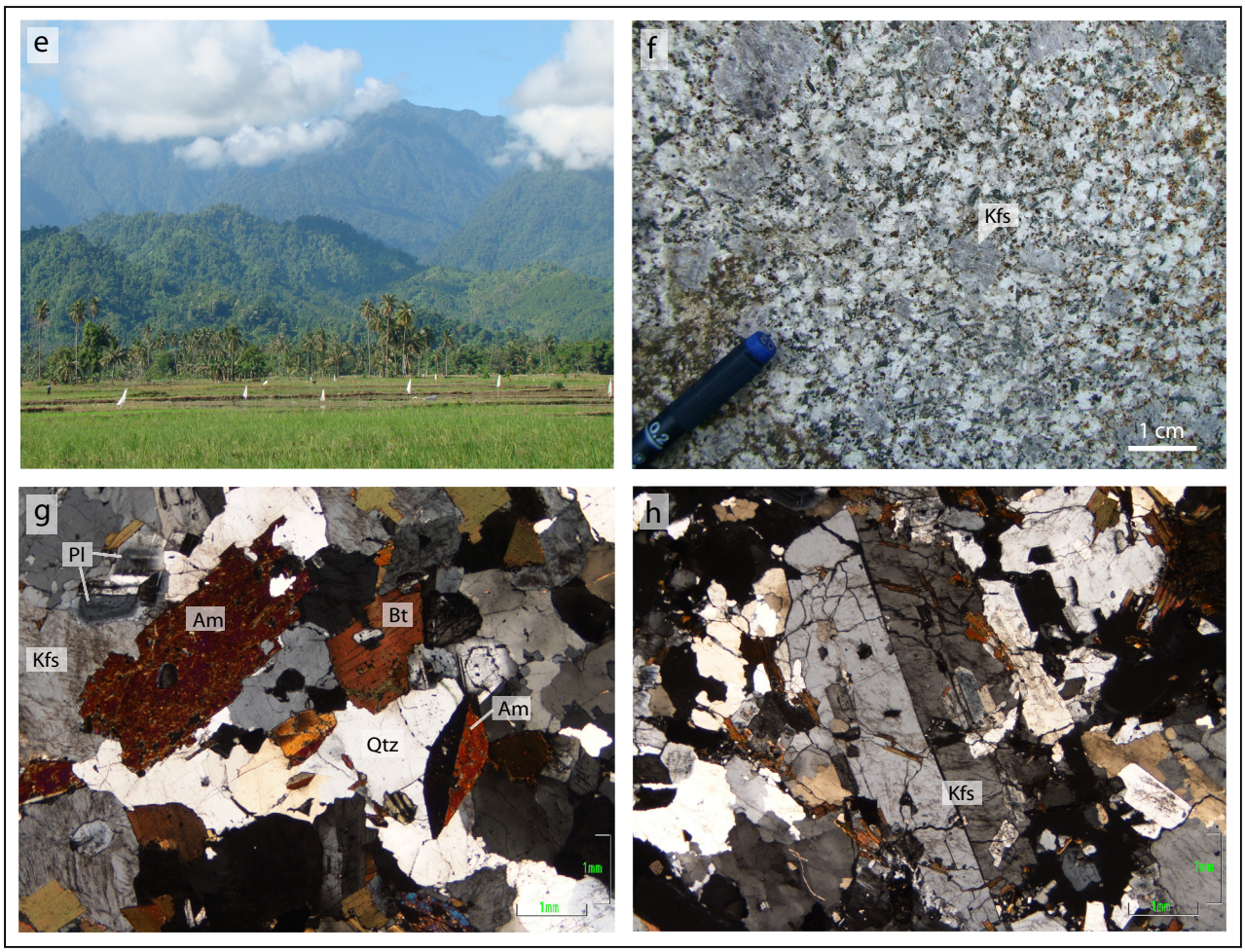
e
f
Kfs
1 cm
g
Pl
Am
Bt
Kfs
Am
Qtz
1mm
h
Kfs

Fig. 4

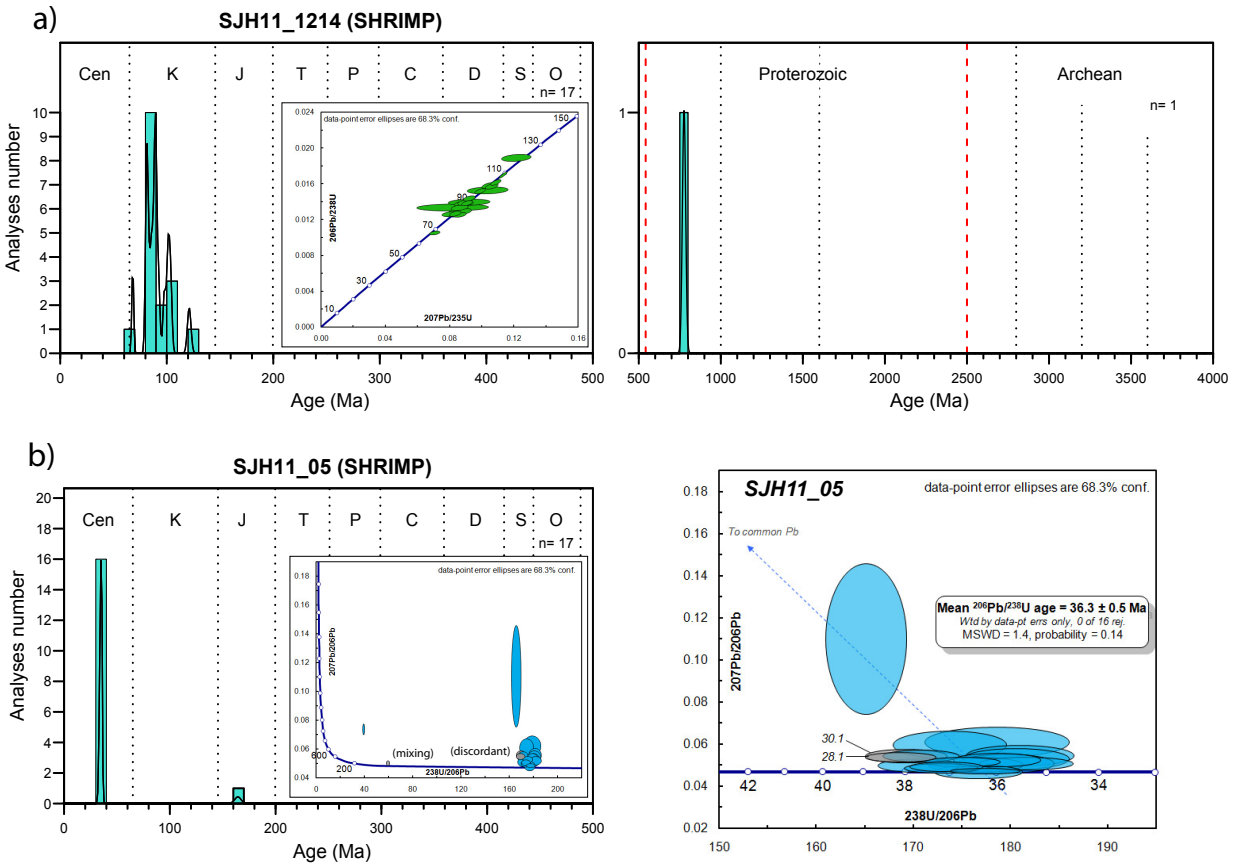
a)
SJH11_1214 (SHRIMP)
Cen
K
J
T
P
C
D
S
O
n= 17
Analyses number
Age (Ma)
data-point error ellipses are 68.3% conf.
206Pb/238U
207Pb/235U
Proterozoic
Archean
n= 1
b)
SJH11_05 (SHRIMP)
SJH11_05
data-point error ellipses are 68.3% conf.
To common Pb
Mean 206Pb/238U age = 36.3 ± 0.5 Ma
Wtd by data-pt errs only, 0 of 16 rej.
MSWD = 1.4, probability = 0.14
207Pb/206Pb
238U/206Pb
(mixing)
(discordant)

Fig. 5

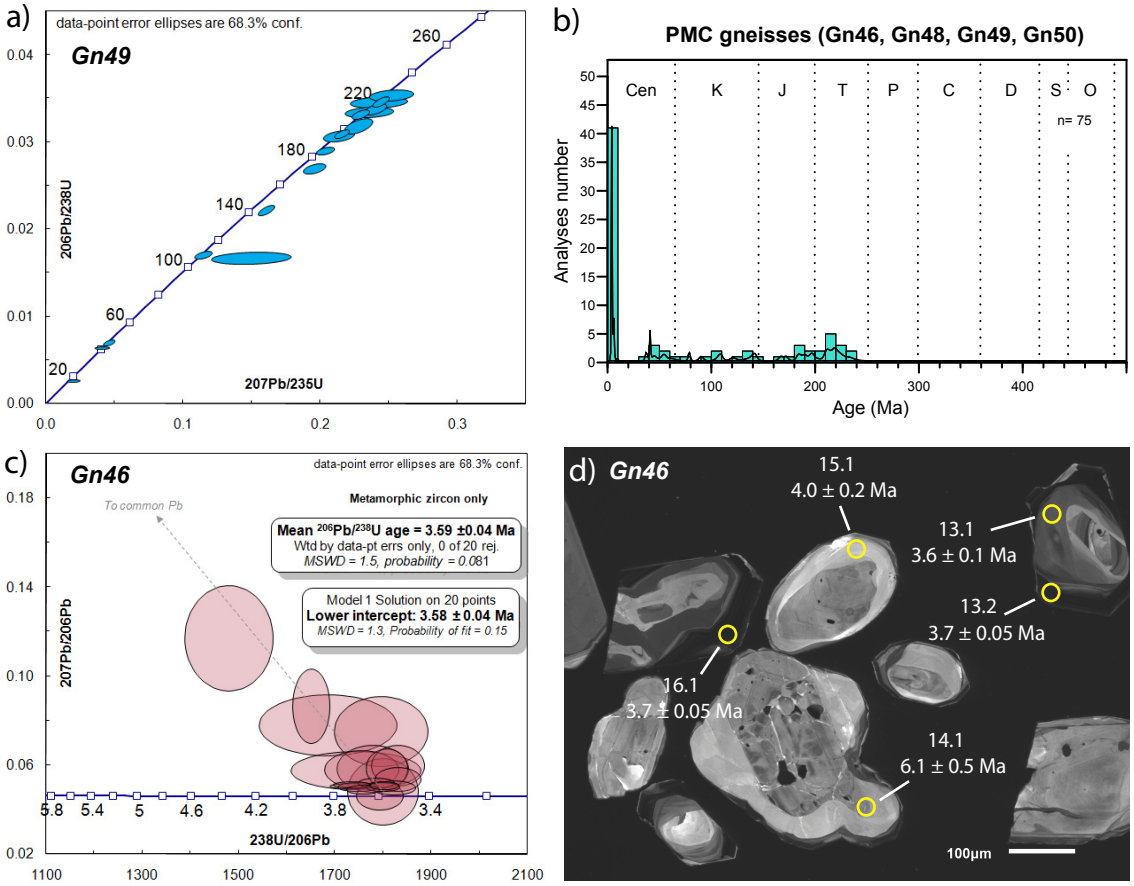
a)
data-point error ellipses are 68.3% conf.
Gn49
206Pb/238U
207Pb/235U
b)
PMC gneisses (Gn46, Gn48, Gn49, Gn50)
Cen
K
J
T
P
C
D
S
O
n= 75
Analyses number
Age (Ma)
c)
Gn46
data-point error ellipses are 68.3% conf.
Metamorphic zircon only
To common Pb
Mean 206Pb/238U age = 3.59 ±0.04 Ma
Wtd by data-pt errs only, 0 of 20 rej.
MSWD = 1.5, probability = 0.081
Model 1 Solution on 20 points
Lower intercept: 3.58 ±0.04 Ma
MSWD = 1.3, Probability of fit = 0.15
207Pb/206Pb
238U/206Pb
d) Gn46
15.1
4.0 ± 0.2 Ma
13.1
3.6 ± 0.1 Ma
13.2
3.7 ± 0.05 Ma
16.1
3.7 ± 0.05 Ma
14.1
6.1 ± 0.5 Ma
100µm

Fig. 6

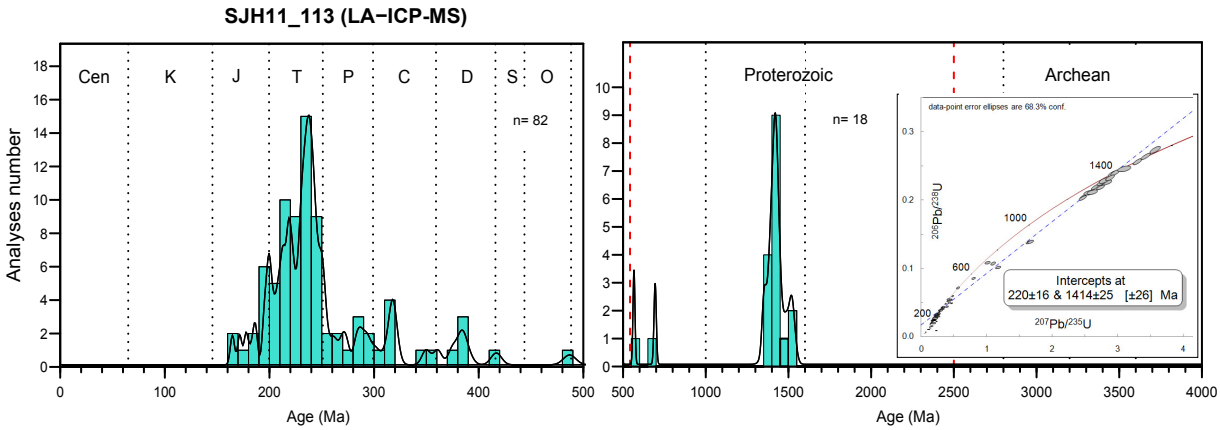
SJH11_113 (LA−ICP-MS)
Cen
K
J
T
P
C
D
S
O
n= 82
Analyses number
Age (Ma)
Proterozoic
Archean
n= 18
data-point error ellipses are 68.3% conf.
1400
1000
600
200
Intercepts at
220±16 & 1414±25 [±26] Ma
206Pb/238U
207Pb/235U
Age (Ma)

Fig. 7

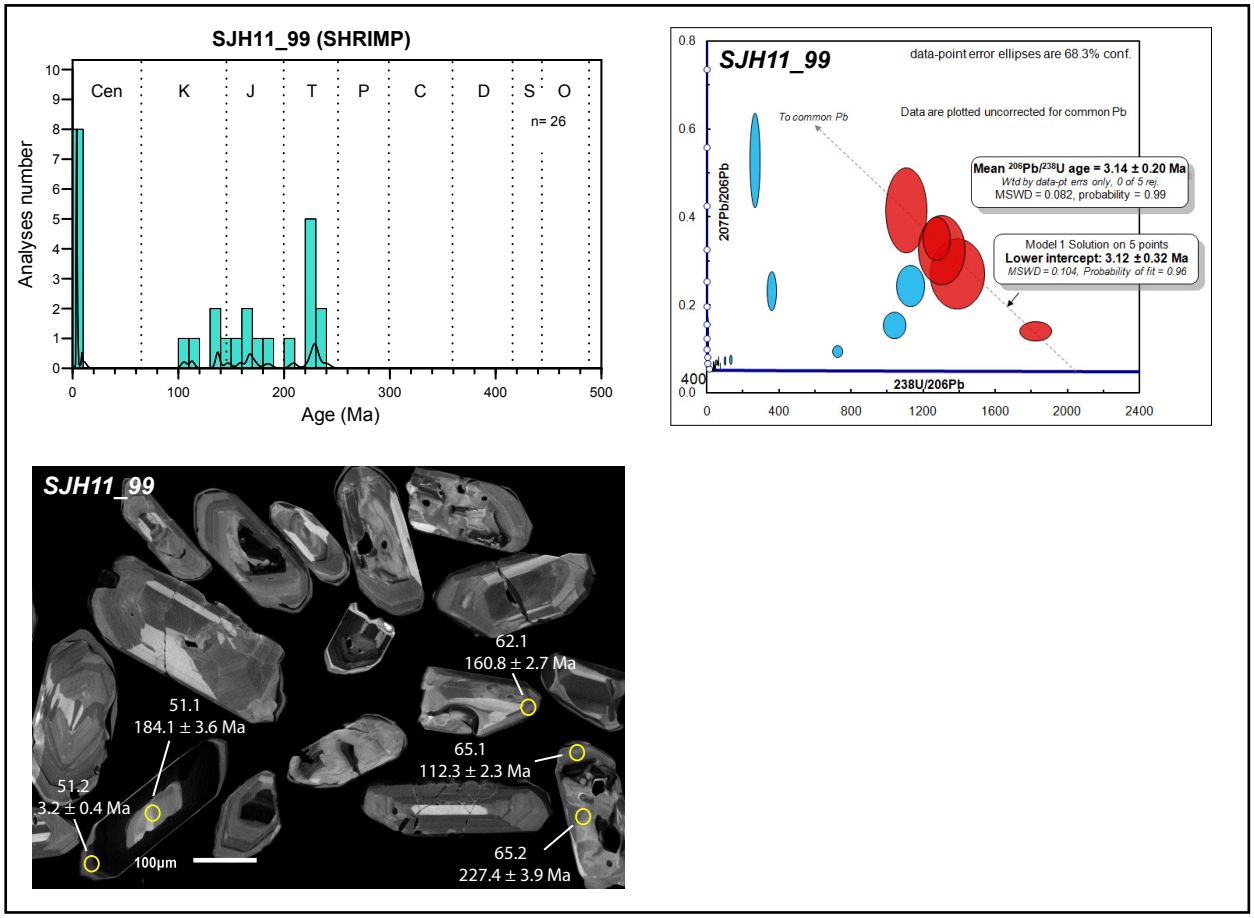
SJH11_99 (SHRIMP)
Cen
K
J
T
P
C
D
S
O
n= 26
Analyses number
Age (Ma)
SJH11_99
data-point error ellipses are 68.3% conf.
To common Pb
Data are plotted uncorrected for common Pb
Mean 206Pb/238U age = 3.14 ± 0.20 Ma
Wtd by data-pt errs only, 0 of 5 rej.
MSWD = 0.082, probability = 0.99
Model 1 Solution on 5 points
Lower intercept: 3.12 ± 0.32 Ma
MSWD = 0.104, Probability of fit = 0.96
207Pb/206Pb
238U/206Pb
SJH11_99
62.1
160.8 ± 2.7 Ma
51.1
184.1 ± 3.6 Ma
65.1
112.3 ± 2.3 Ma
51.2
3.2 ± 0.4 Ma
65.2
227.4 ± 3.9 Ma
100μm

Fig. 8

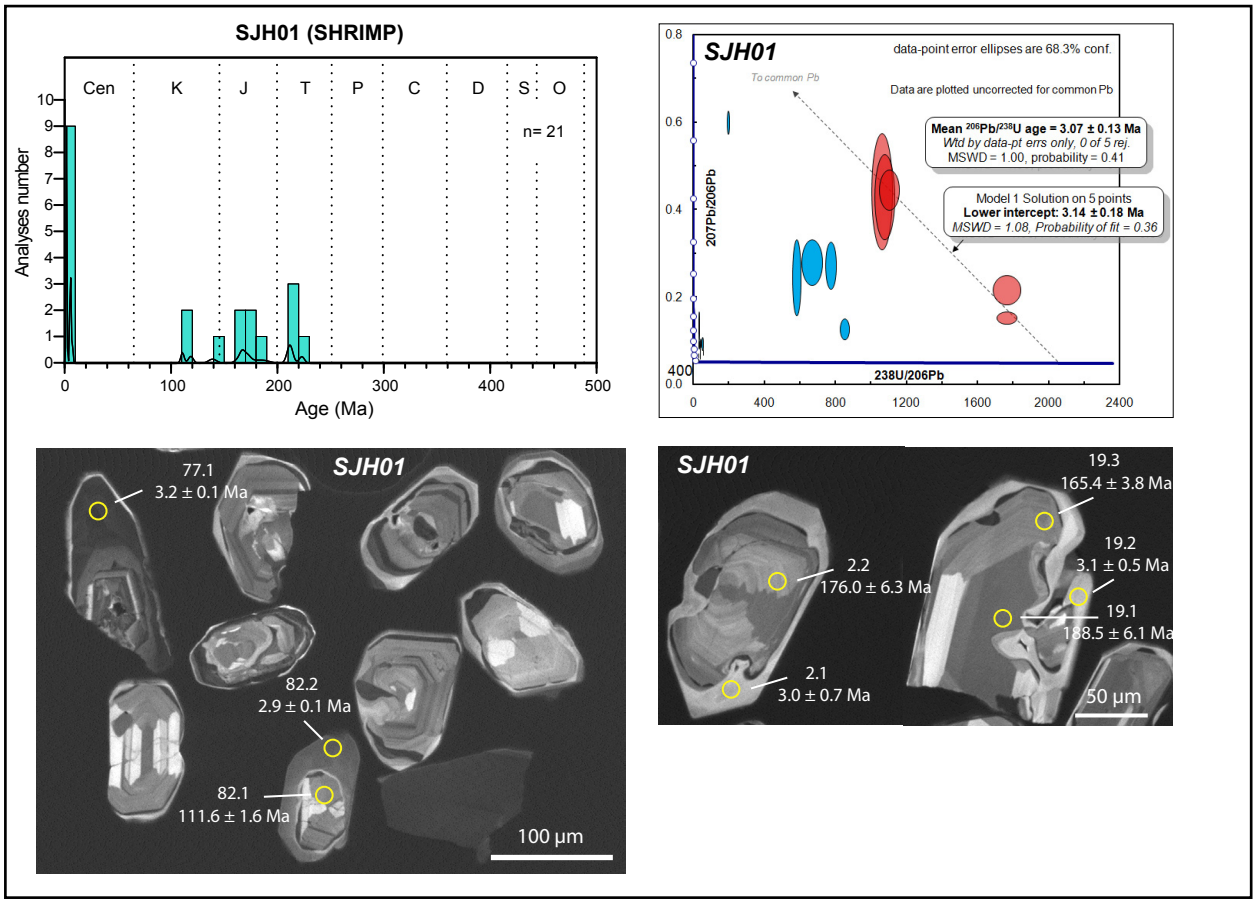
SJH01 (SHRIMP)
Cen
K
J
T
P
C
D
S
O
n= 21
Analyses number
Age (Ma)
SJH01
data-point error ellipses are 68.3% conf.
To common Pb
Data are plotted uncorrected for common Pb
Mean 206Pb/238U age = 3.07 ± 0.13 Ma
Wtd by data-pt errs only, 0 of 5 rej.
MSWD = 1.00, probability = 0.41
Model 1 Solution on 5 points
Lower intercept: 3.14 ± 0.18 Ma
MSWD = 1.08, Probability of fit = 0.36
207Pb/206Pb
238U/206Pb
SJH01
77.1
3.2 ± 0.1 Ma
82.2
2.9 ± 0.1 Ma
82.1
111.6 ± 1.6 Ma
100 µm
SJH01
2.2
176.0 ± 6.3 Ma
2.1
3.0 ± 0.7 Ma
19.3
165.4 ± 3.8 Ma
19.2
3.1 ± 0.5 Ma
19.1
188.5 ± 6.1 Ma
50 µm

Fig. 9

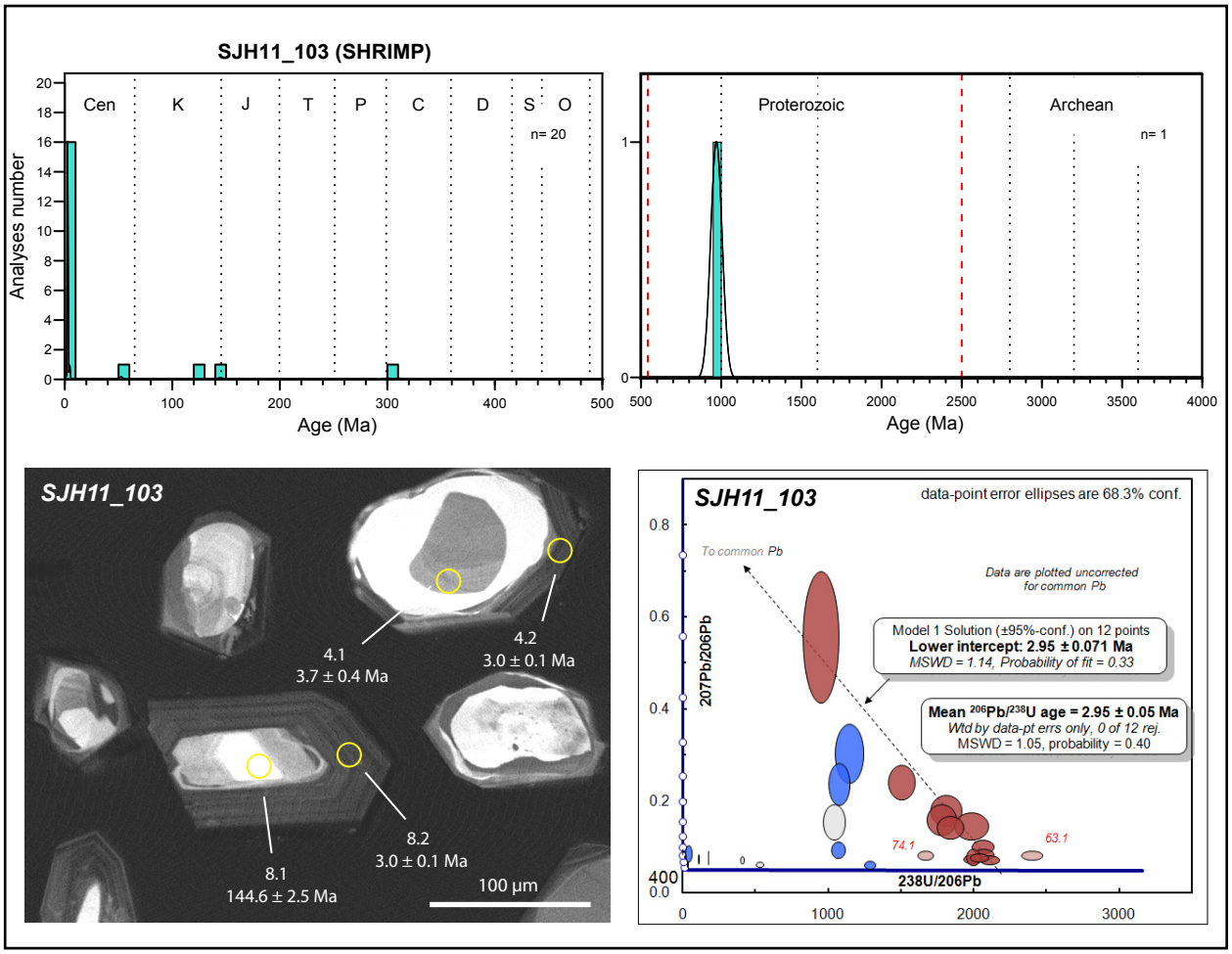
SJH11_103 (SHRIMP)
Cen
K
J
T
P
C
D
S
O
n= 20
Analyses number
Age (Ma)
Proterozoic
Archean
n= 1
Age (Ma)
SJH11_103
4.1
3.7 ± 0.4 Ma
4.2
3.0 ± 0.1 Ma
8.1
144.6 ± 2.5 Ma
8.2
3.0 ± 0.1 Ma
100 µm
SJH11_103
data-point error ellipses are 68.3% conf.
To common Pb
Data are plotted uncorrected for common Pb
Model 1 Solution (±95%-conf.) on 12 points
Lower intercept: 2.95 ± 0.071 Ma
MSWD = 1.14, Probability of fit = 0.33
Mean 206Pb/238U age = 2.95 ± 0.05 Ma
Wtd by data-pt errs only, 0 of 12 rej.
MSWD = 1.05, probability = 0.40
207Pb/206Pb
238U/206Pb
74.1
63.1

Fig. 10

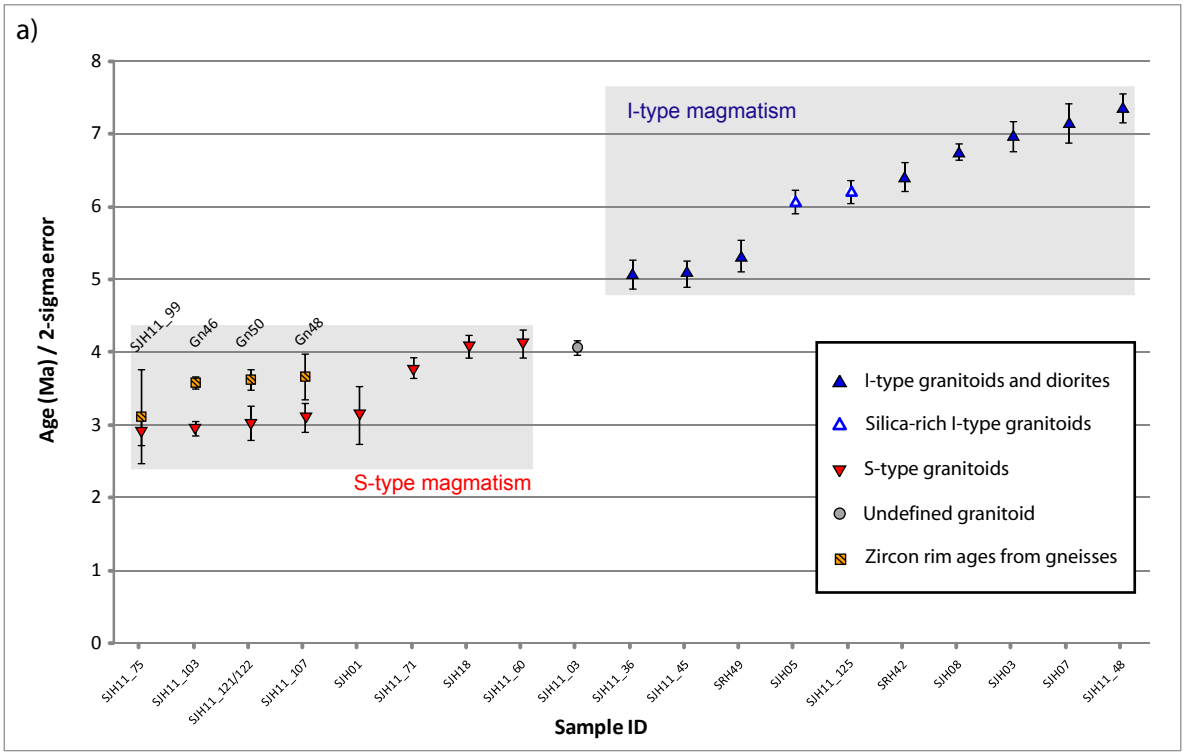
a)
Age (Ma) / 2-sigma error
Sample ID
I-type magmatism
S-type magmatism
SJH11_99
Gn46
Gn50
Gn48
I-type granitoids and diorites
Silica-rich I-type granitoids
S-type granitoids
Undefined granitoid
Zircon rim ages from gneisses
SJH11_75
SJH11_103
SJH11_121/122
SJH11_107
SJH01
SJH11_71
SJH18
SJH11_60
SJH11_03
SJH11_36
SJH11_45
SRH49
SJH05
SJH11_125
SRH42
SJH08
SJH03
SJH07
SJH11_48

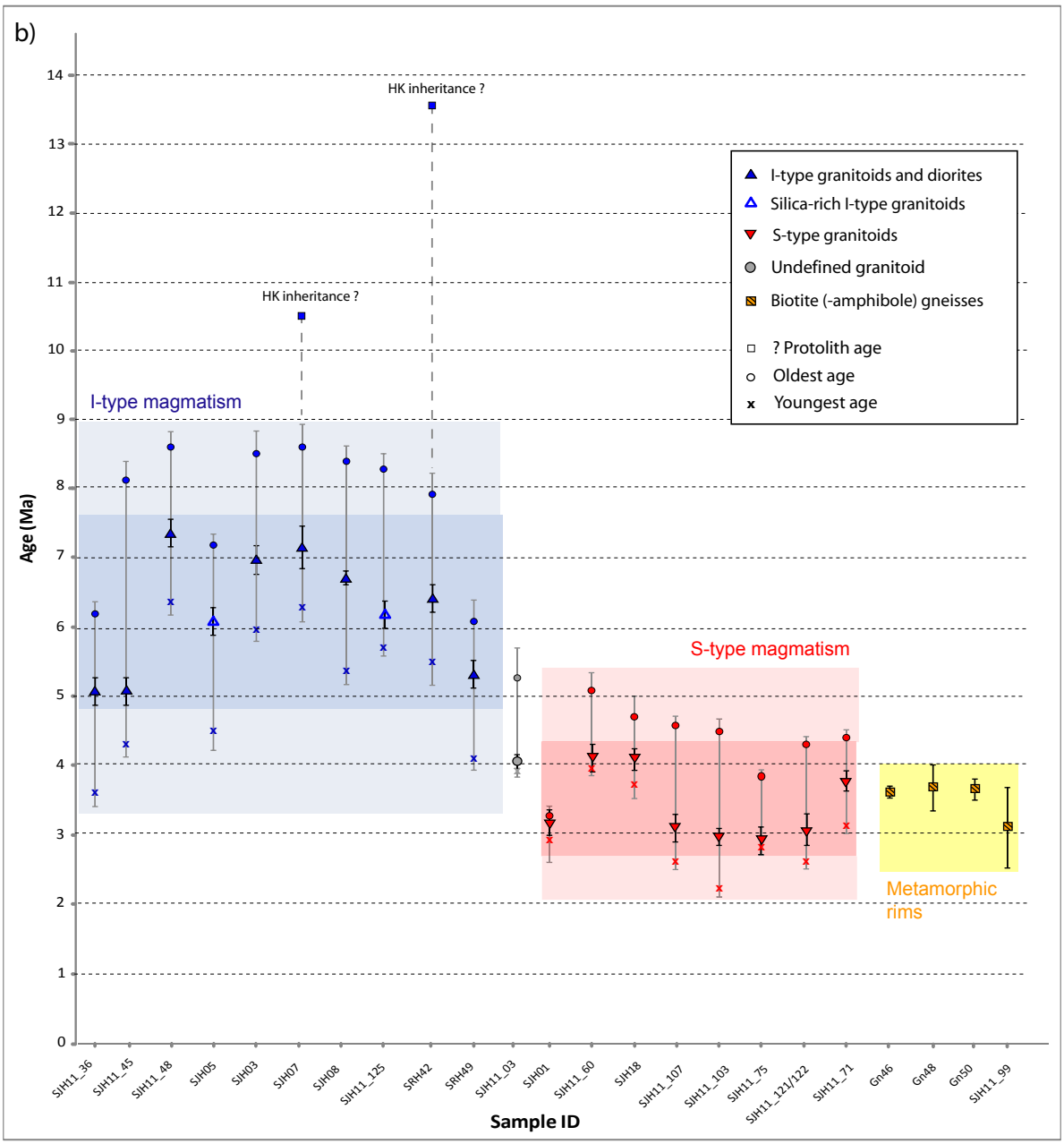
b)
Age (Ma)
Sample ID
HK inheritance ?
HK inheritance ?
I-type magmatism
S-type magmatism
Metamorphic rims
I-type granitoids and diorites
Silica-rich I-type granitoids
S-type granitoids
Undefined granitoid
Biotite (-amphibole) gneisses
? Protolith age
Oldest age
Youngest age
SJH11_36
SJH11_45
SJH11_48
SJH05
SJH03
SJH07
SJH08
SJH11_125
SRH42
SRH49
SJH11_03
SJH01
SJH11_60
SJH18
SJH11_107
SJH11_103
SJH11_75
SJH11_121/122
SJH11_71
Gn46
Gn48
Gn50
SJH11_99

Fig. 11

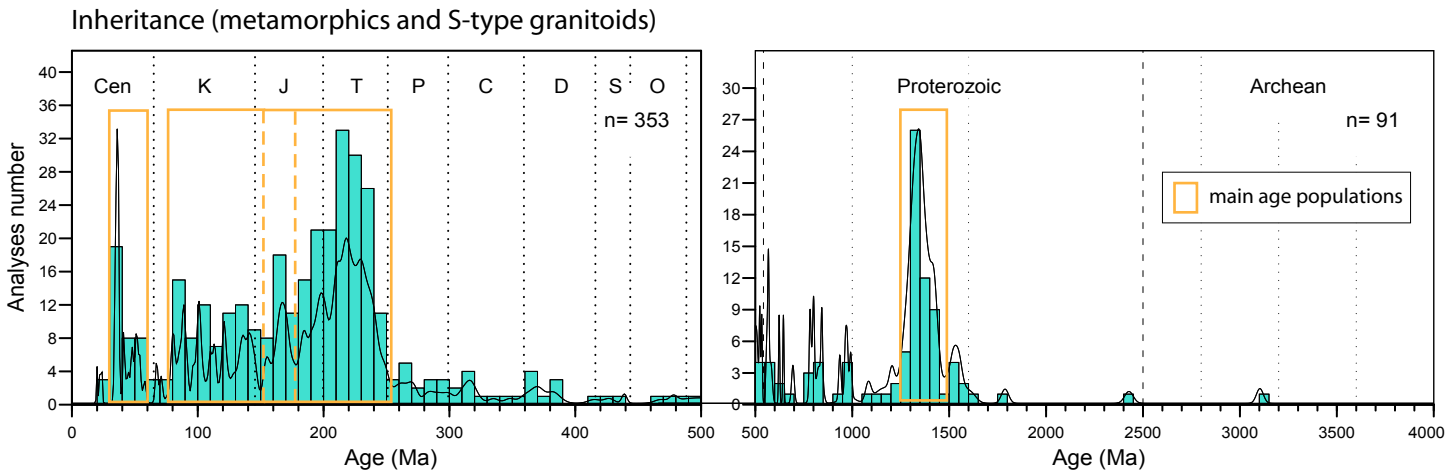
Inheritance (metamorphics and S-type granitoids)
Analyses number
Cen
K
J
T
P
C
D
S
O
n= 353
Age (Ma)
Proterozoic
Archean
n= 91
main age populations
Age (Ma)

Fig. 12

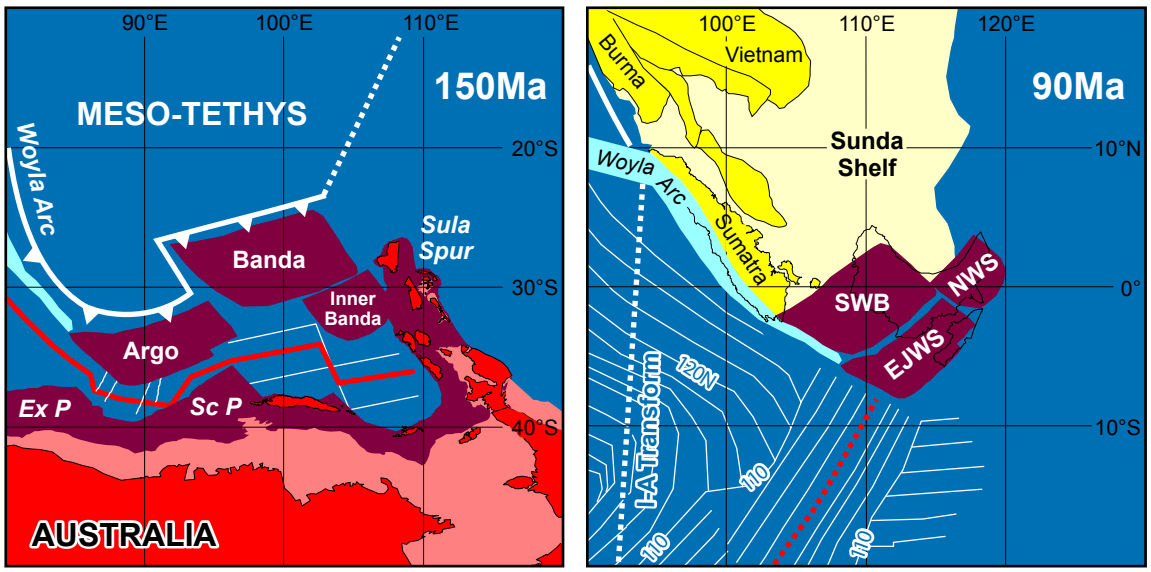
90°E
100°E
110°E
150Ma
MESO-TETHYS
20°S
30°S
40°S
Woyla Arc
Banda
Sula
Spur
Inner
Banda
Argo
Ex P
Sc P
AUSTRALIA
100°E
110°E
120°E
90Ma
Burma
Vietnam
Sunda
Shelf
10°N
0°
10°S
Woyla Arc
Sumatra
SWB
NWS
EJWS
120N
110
110
110
IA Transform

Fig. 13

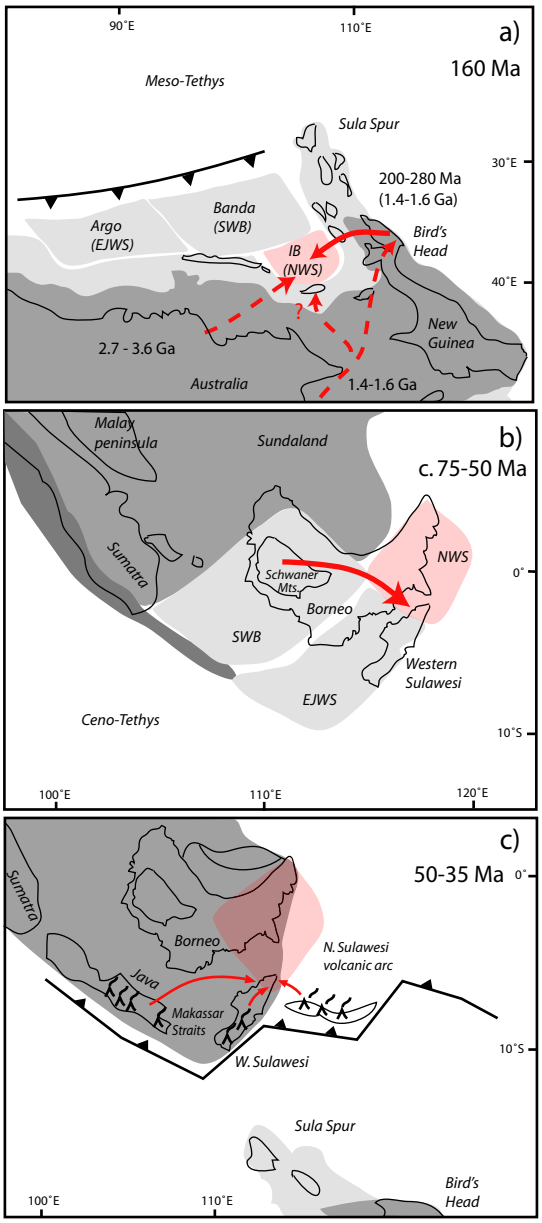
a)
160 Ma
90°E
110°E
30°E
40°E
Meso-Tethys
Sula Spur
200-280 Ma
(1.4-1.6 Ga)
Banda
(SWB)
Argo
(EJWS)
IB
(NWS)
Bird's
Head
New
Guinea
2.7 - 3.6 Ga
Australia
1.4-1.6 Ga
b)
c. 75-50 Ma
Malay
peninsula
Sundaland
Sumatra
NWS
Schwaner
Mts
Borneo
SWB
Western
Sulawesi
EJWS
Ceno-Tethys
0°
10°S
100°E
110°E
120°E
c)
50-35 Ma
0°
Sumatra
Borneo
N. Sulawesi
volcanic arc
Java
Makassar
Straits
W. Sulawesi
10°S
Sula Spur
Bird's
Head
100°E
110°E

Fig. 14

Sample ID	Location	Lithology	Formation	Type	SHRIMP					LA-ICP-MS								
Metamorphic rocks					No. core analyses	No. rim analyses	No. inheritance	Mean age (Ma)/ ±1σ	MSWD	No. analyses	No. conc./disc.				Upper intercept - Mean age (Ma)/ ±1σ	Lower intercept - Mean age (Ma)/ ±1σ		
SJH11_05	Neck	Schist	Metamorphic rocks (PMC)	Outcrop	15	2	17	**36.3 ± 0.5**	1.4									
SJH11_1214	Neck	Schist	Metamorphic rocks (PMC)	Outcrop	15	3	18	-	-									
Gn46	Neck	Gneiss	Metamorphic rocks (PMC)	Boulder	2	24	2	**3.59 ± 0.04**	1.5									
Gn48	Neck	Gneiss	Metamorphic rocks (PMC)	Outcrop	3	11	8	**3.67 ± 0.16**	0.72									
Gn49	Neck	Gneiss	Metamorphic rocks (PMC)	Boulder	7	9	16	-	-									
Gn50	Neck	Gneiss	Metamorphic rocks (PMC)	Outcrop	5	14	8	**3.63 ± 0.07**	0.94									
SJH28	mid Sulawesi	Gneiss	Metamorphic rocks	Boulder						74	58/16				**1336.1 ± 9.5**	-		
SJH11_99	mid Sulawesi	Gneiss	Metamorphic rocks	Boulder	9	17	18	**3.12 ± 0.32**	0.10	79	60/19							
SJH11_113	mid Sulawesi	Gneiss	Metamorphic rocks	Boulder	12	7	16	-	-	122	100/22				**1417.0 ± 11.0**	**234.7 ± 2.0**		
Magmatic rocks										No. analyses	No. inheritance (conc./disc.)	Mean age - reject (outlier)	Mean age - reject (unmix)	No. mean age calc.	Mean age (Ma)/ ±1σ	MSWD	relative fraction	
SJH01	Neck	Granite dyke	Neogene granitoids and diorites	Outcrop	12	9	12	**3.14 ± 0.18**	1.08	73	23/41	-	-	-	-	-	-	
SJH03	Neck	Granodiorite	Neogene granitoids and diorites	Outcrop						75	-	8	-	67	**6.97 ± 0.10**	9.7	1.00	
SJH05	Neck	Granite	Neogene granitoids and diorites	Outcrop						24	1/-	5	8	10	**6.08 ± 0.08**	0.9	0.56	
SJH06	Neck	Granodiorite	Paleogene intrusives	Boulder	13	4	2	**35.14 ± 0.52**	0.59	58/28*	6/2	-	4	18	**35.16 ± 0.65**	2.1	0.82	
SJH07	mid Sulawesi	Diorite	Neogene granitoids and diorites	Boulder						63	-	4	-	59	**7.15 ± 0.13**	6.2	1.00	
SJH08	mid Sulawesi	Granodiorite	Neogene granitoids and diorites	Boulder						64	-	18	-	46	**6.74 ± 0.07**	5.0	1.00	
SJH18	mid Sulawesi	Granodiorite	Neogene granitoids and diorites	Outcrop						62	16/14	11	-	21	**4.07 ± 0.08**	2.0	1.00	
SJH11_03	Neck	Granite	Neogene granitoids and diorites	Boulder						51	-/5	10	21	15	**4.06 ± 0.05**	0.9	0.42	
SJH11_10	Neck	Microgranite	Paleogene intrusives	Outcrop						43/12*	2/2	-	4	6	**33.10 ± 1.10**	1.7	0.60	
SJH11_36	Neck	Granodiorite	Neogene granitoids and diorites	Outcrop						57	1/1	10	-	45	**5.07 ± 0.10**	2.4	1.00	
SJH11_45	Neck	Granodiorite	Neogene granitoids and diorites	Boulder						40	-	7	16	17	**5.08 ± 0.09**	1.8	0.52	
SJH11_48	Neck	Granodiorite	Neogene granitoids and diorites	Boulder						38	1/-	11	-	26	**7.36 ± 0.09**	3.6	1.00	
SJH11_60	mid Sulawesi	Granite	Neogene granitoids and diorites	Outcrop						29	9/1	3	6	10	**4.12 ± 0.10**	1.4	0.63	
SJH11_71	mid Sulawesi	Granodiorite	Neogene granitoids and diorites	Outcrop						45	3/3	5	9	25	**3.78 ± 0.07**	2.9	0.74	
SJH11_75	mid Sulawesi	Granite	Neogene granitoids and diorites	Boulder						44	15/11	2	8	8	**2.92 ± 0.08**	0.8	0.50	
SJH11_103	mid Sulawesi	Granite	Neogene granitoids and diorites	Outcrop	5	16	5	**2.95 ± 0.07**	1.14	52	13/14	7	-	18	**2.53 ± 0.10**	3.7	1.00	
SJH11_107	mid Sulawesi	Granite	Neogene granitoids and diorites	Outcrop						46	15/14	1	11	5	**3.11 ± 0.10**	0.5	0.31	
SJH11_121/122	mid Sulawesi	Granodiorite	Neogene granitoids and diorites	Outcrop						52	15/5	7	8	17	**3.05 ± 0.12**	4.6	0.68	
SJH11_125	mid Sulawesi	Granodiorite	Neogene granitoids and diorites	Outcrop						60	2/-	7	21	30	**6.21 ± 0.08**	2.7	0.59	
SRH42	mid Sulawesi	Granodiorite	Neogene granitoids and diorites	Outcrop						61	3/-	8	25	25	**6.41 ± 0.09**	0.8	0.50	
SRH49	mid Sulawesi	Syenite	Neogene granitoids and diorites	Boulder						24	-	3	-	21	**5.32 ± 0.11**	2.7	1.00	

* Number of concordant analyses.

calc. = calculation; conc. = concordant; disc. = discordant; No. = number.

Neogene granitoids and diorites

Group	CA	HK	CAK						
Area	PKF	PKF	Neck	Neck	Neck	Neck	Neck	Neck	Neck
Sample	**SJH17**	**SJH07**	**SJH01**	**SJH03**	**SJH04**	**SJH11_15**	**SJH11_35**	**SJH11_36**	**SJH11_45**
Rock type	D	D	GRA	GRD	GRA	GRD	GRA	GRD	GRD
Character	I-type	I-type	S-type	I-type	silica-rich I-type	S-type	S-type	I-type	I-type
SiO_2	59.74	58.71	74.18	64.81	70.07	69.30	70.58	66.46	66.94
TiO_2	0.47	0.87	0.13	0.58	0.29	0.42	0.31	0.60	0.54
Al_2O_3	21.88	16.91	14.21	15.40	15.55	16.04	15.22	14.84	14.59
Fe_2O_3	2.52	5.85	1.03	3.75	1.60	2.10	1.75	3.52	3.43
MnO	0.04	0.10	0.04	0.07	0.05	0.03	0.04	0.07	0.07
MgO	1.64	4.03	0.27	2.45	0.78	0.77	0.84	2.25	2.22
CaO	7.17	6.22	1.40	3.90	1.86	2.42	1.96	3.02	2.97
Na_2O	4.48	3.02	3.64	2.91	3.66	3.33	3.78	3.35	3.25
K_2O	1.51	3.24	4.15	4.32	5.54	4.93	5.00	5.10	5.21
P_2O_5	0.13	0.30	0.05	0.19	0.15	0.13	0.15	0.37	0.37
SO_3	0.03	0.01	0.01	0.01	0.03	0.03	0.02	0.02	0.02
LOI	0.40	0.50	0.28	0.60	0.36	0.65	0.44	0.48	1.01
Total	99.61	99.27	99.12	98.38	99.59	99.50	99.64	99.61	99.61
Ni	14	22	3	15	8	7	13	30	32
Cr	82	144	4	102	20	12	26	74	90
V	65	110	9	69	21	37	29	86	77
Sc	6	18	3	10	4	5	6	11	10
Cu	7	11	3	5	5	3	5	6	8
Ga	23	21	16	17	20	18	18	18	18
Pb	30	26	58	40	106	57	62	37	43
Sr	758	463	283	328	495	366	741	563	652
Rb	60	146	207	189	398	206	218	204	215
Ba	580	865	613	704	977	737	1361	1561	1514
Zr	71	192	71	127	173	174	174	173	182
Nb	7	18	10	14	23	12	17	16	16
Ta	<0.4	0.6	1.7	1.3	2.3	1.1	1.6	1.0	1.1
Mo	<0.4	<0.4	<0.4	<0.4	<0.4	<0.4	<0.4	<0.4	<0.4
Th	3	14	14	14	24	30	27	19	28
U	1.1	2.5	4.2	3.9	16.8	5.5	9.6	6.0	7.2
Y	8	25	15	23	13	15	15	21	20
La	20	30	11	29	26	36	26	36	38
Ce	29	62	25	59	54	71	52	69	73
Nd	12	28	11	25	21	27	22	28	29
Sm	<1.8	6.2	4.0	6.1	4.1	5.2	2.9	3.4	5.5
Yb	1.4	2.0	1.3	2.0	0.7	1.3	<0.5	1.3	1.9
Cs	2	5	7	10	27	5	4	5	4

All iron is measured as Fe_2O_3. LOI = loss on ignition (wt %). Oxides in wt %; elements in ppm.

PKF = Palu-Koro Fault; D = diorite; GRD = granodiorite; GRA = granite.

Table 2

Neogene granitoids and diorites

Group	CAK									
Area	PKF	PKF	PKF	PKF	E of PKF	E of PKF	E of PKF	E of PKF	E of PKF	E of PKF
Sample	**SJH08**	**SJH14**	**SJH11_71**	**SJH11_75**	**SJH18**	**SJH26**	**SJH11_94**	**SJH11_95**	**SJH11_121**	**SJH11_125**
Rock type	GRD	GRA	GRD	GRA	GRD	GRA	GRA	GRA	GRD	GRD
Character	I-type	S-type	S-type	S-type	S-type	S-type	S-type	S-type	S-type	ilica-rich I-type
SiO_2	66.11	75.28	70.43	72.20	69.76	71.03	75.82	70.63	71.71	66.85
TiO_2	0.49	0.08	0.41	0.37	0.54	0.19	0.17	0.30	0.37	0.58
Al_2O_3	15.47	14.06	15.06	15.02	15.81	15.48	12.94	15.57	14.86	15.84
Fe_2O_3	3.59	0.31	2.33	1.91	3.16	1.37	1.16	1.89	1.82	3.42
MnO	0.07	0.01	0.04	0.03	0.04	0.03	0.03	0.05	0.03	0.07
MgO	2.38	0.10	1.01	0.63	1.11	0.43	0.15	0.70	0.72	2.00
CaO	3.76	0.98	2.53	1.25	2.74	1.62	0.78	1.98	1.96	3.32
Na_2O	2.99	3.78	3.53	2.75	3.62	4.00	3.14	4.12	3.36	2.93
K_2O	4.54	5.48	3.70	5.28	2.46	4.83	5.43	4.27	4.64	4.41
P_2O_5	0.22	0.01	0.15	0.14	0.08	0.05	0.01	0.10	0.14	0.18
SO_3	0.01	0.01	0.01	0.03	0.01	0.01	0.02	0.02	0.02	0.02
LOI	0.47	0.22	0.46	1.40	0.57	0.38	0.28	0.57	0.46	0.79
Total	99.63	100.10	99.20	99.60	99.34	99.02	99.65	99.63	99.62	99.61
Ni	22	4	9	5	13	6	3	8	5	18
Cr	90	4	20	10	24	8	2	12	10	70
V	71	7	46	23	53	17	11	26	27	58
Sc	11	2	8	6	8	3	3	4	5	10
Cu	7	24	6	4	6	8	3	6	3	13
Ga	18	17	18	20	18	17	13	18	19	21
Pb	50	79	49	59	44	95	6	92	54	109
Sr	487	424	466	244	484	953	120	885	316	321
Rb	196	230	194	308	99	201	186	165	287	220
Ba	904	1088	638	648	679	2427	473	1501	566	705
Zr	162	83	148	165	279	135	64	173	160	190
Nb	18	23	13	15	9	16	7	14	12	15
Ta	2.1	1.4	1.9	2.1	<0.4	0.7	0.4	1.2	1.4	1.0
Mo	<0.4	<0.4	<0.4	<0.4	<0.4	<0.4	<0.4	<0.4	<0.4	<0.4
Th	21	23	20	29	42	26	3	28	25	20
U	6.0	10.1	6.1	6.9	5.0	8.3	0.9	7.5	5.8	6.3
Y	20	7	16	22	12	13	9	13	20	21
La	26	11	24	33	53	24	12	32	25	31
Ce	56	22	51	65	101	48	21	61	55	63
Nd	25	8	20	26	36	18	9	23	23	26
Sm	6.2	2.7	2.4	4.8	6.2	1.9	<1.8	3.5	5.9	5.7
Yb	1.8	0.7	1.0	1.6	1.0	0.9	1.5	0.6	1.9	2.3
Cs	8	5	13	21	4	3	<1	5	19	17

All iron is measured as Fe_2O_3. LOI = loss on ignition (wt %). Oxides in wt %; elements in ppm.

PKF = Palu-Koro Fault; D = diorite; GRD = granodiorite; GRA = granite.

Table 2 *(cont.)*